A&A 462, 107–122 (2007)
DOI: 10.1051/0004-6361:20054197

Astronomy & Astrophysics

Monte Carlo simulations of metal-poor star clusters[⋆,⋆⋆]

M. Fagiolini[1,2], G. Raimondo[3], and S. Degl'Innocenti[1,2]

[1] Dipartimento di Fisica, Università di Pisa, Largo B. Pontecorvo 3, 56126 Pisa, Italy
e-mail: raimondo@oa-teramo.inaf.it
[2] INFN, Sezione di Pisa, Largo B. Pontecorvo 3, 56126 Pisa, Italy
[3] INAF, Osservatorio Astronomico di Teramo, via M. Maggini, 64100 Teramo, Italy

Received 13 September 2005 / Accepted 7 August 2006

ABSTRACT

Context. Metal-poor globular clusters (GCs) can provide a probe of the earliest epoch of star formation in the Universe, being the oldest observable stellar systems. In addition, young and intermediate-age low-metallicity GCs are present in external galaxies. Nevertheless, inferring their evolutionary status by using integrated properties may suffer from large *intrinsic* uncertainty caused by the discrete nature of stars in stellar systems, especially in the case of faint objects.
Aims. In this paper, we evaluate the *intrinsic* uncertainty (due to statistical effects) affecting the integrated colours and mass-to-light ratios as a function of the cluster's integrated visual magnitude ($M_V^{\rm tot}$), which represents a directly measured quantity. We investigate the case of metal-poor, single-burst stellar populations with age from a few million years to a likely upper value for the Galactic globular cluster ages (~15 Gyr).
Methods. Our approach is based on Monte Carlo techniques for randomly generating stars distributed according to the cluster's mass function.
Results. Integrated colours and mass-to-light ratios in different photometric bands are checked for good agreement with the observational values of low-metallicity Galactic clusters; the effect of different assumptions on the horizontal branch (HB) morphology is shown to be irrelevant, at least for the photometric bands explored here. We present integrated colours and mass-to-light ratios as a function of age for different assumptions on the cluster total V magnitude. We find that the *intrinsic* uncertainty cannot be neglected. In particular, in models with $M_V^{\rm tot} = -4$ the broad-band colours show an *intrinsic* uncertainty high enough to prevent the precise age of the cluster from being evaluated. The effects of different assumptions on the initial mass function and on the minimum mass for which carbon burning is ignited for both integrated colours and mass-to-light ratios are also analysed. Finally, the present predictions are compared with recent results available in the literature, showing non-negligible differences in some cases.

Key words. stars: evolution – Galaxy: globular clusters: general – galaxies: star clusters

1. Introduction

A key issue in astronomy is to determine the ages and chemical compositions of those stars and stellar systems that are needed to reconstruct the formation and evolution of galaxies. Toward this goal, analysing the stellar cluster population in external galaxies and in the Milky Way is fundamental for tracing the history of the parent galaxy (see, e.g. Cote et al. 1998; West et al. 2004). In contrast to the situation in the Galaxy where massive ($\approx 10^5 \div 10^6$ stars) stellar clusters are old ($\gtrsim$10 Gyr) and metal poor ([Fe/H] $\lesssim -0.7$), observations indicate that in the Magellanic Clouds, in the Local Group galaxies, and even in galaxies beyond the Local Group, massive stellar clusters offer a wide range of both metallicity and age, so they are considered the main indicators of stellar formation events in the galaxies history (Larsen 2000; Matteucci et al. 2002; Harris 2003). We use the term "globular clusters" (GCs) to signify the massive clusters of any given age and chemical composition.

GCs have the advantage of being bright objects and then of being easily observed beyond the Local Group. In addition, they are thought to be simple stellar populations (SSPs) consisting of a gravitationally bound group of stars born at nearly the same moment and with a nearly identical chemical composition. The integrated broad-band colours, line indices, and mass-to-light ratios that we observe from those systems are the unique observational tools for understanding their properties. Since the pioneering work by Tinsley (1972), different groups have developed population synthesis models for interpreting these observables: e.g. Renzini & Buzzoni (1986), Brocato et al. (1990b), Charlot & Bruzual (1991), Buzzoni (1993), Bressan et al. (1994), Worthey (1994), Maraston (1998), Kurth et al. (1999), Brocato et al. (2000), Vazdekis (1999), Girardi et al. (2000), Anders & Fritze-v. Alvensleben (2003), Bruzual & Charlot (2003), and Maraston (2005).

Besides the *systematic* uncertainties due to different sets of stellar evolutionary tracks and different spectral libraries used to transform the models from luminosity and effective temperature to observable quantities (see e.g. Charlot et al. 1996; Maraston 1998; Brocato et al. 2000; Bruzual & Charlot 2003; Yi 2003), broad-band colours may suffer from large *intrinsic* fluctuations caused by the discrete nature of the number of stars in the system. The first studies were carried out in the optical by Barbaro & Bertelli (1977) for population I clusters and

⋆ Full Tables 2, 3 and 6 are only available in electronic form at the CDS via anonymous ftp to cdsarc.u-strasbg.fr (130.79.128.5) or via
http://cdsweb.u-strasbg.fr/cgi-bin/qcat?J/A+A/462/107
⋆⋆ All the figures are available as coloured figures in the electronic edition of the Journal.

by Chiosi et al. (1988) for intermediate ($Z = 0.001$) and solar metallicity, while Santos & Frogel (1997) analysed the case for near-infrared (NIR) bands. Among other results, these authors conclude that it is necessary to include stochastic effects when deriving ages and metallicities from integrated broad-band colours.

Most studies normalized their theoretical predictions to the total number of stars or total mass in the cluster, while Brocato et al. (1999, 2000) derived the mean broad-band colours and the corresponding dispersions as a function of the cluster's visual magnitude ($M_V^{\rm tot}$) for selected values of ages. This approach directly links theory and observations and is crucial when the cluster age and metallicity are inferred from the observed broad-band colours, especially for clusters at the faint end of the GC luminosity function.

In this paper we extend the investigations by Brocato et al. (1999) and Brocato et al. (2000) and analyse stochastic effects not only on broad-band colours, but also on mass-to-light ratios as a function of the adopted cluster visual magnitude, $M_V^{\rm tot}$. We provide a comprehensive study of this problem by investigating the time-evolution of both integrated colours and mass-to-light ratios for a fine grid of stellar ages and for three different values of $M_V^{\rm tot}$. The analysis is carried out using new single-burst low-metallicity models ($Z = 0.0002$) based on the updated database of stellar models by Cariulo et al. (2004). We choose this metallicity because the metal-poor GCs can provide a probe of the earliest epoch of star formation in the Universe, being the oldest observable stellar systems. In addition, young and intermediate-age low-metallicity GCs are present in external galaxies (Larsen & Richtler 1999). For these reasons, and also because analysing young metal-poor clusters gives an idea on how old GCs appeared when they formed, we explore a wide range of ages ($7.7 \leq \log[{\rm age(yr)}] \leq 10.3$). We note that we did not take redshift effects into account, so that our calculations can be used only for objects with a redshift lower than about 0.1.

The results are compared with a sample of low-metallicity clusters in the Galaxy with different HB morphology, chosen as prototypes of the old stellar populations studied in this work. The present theoretical predictions are also compared with recent results available in the literature showing in some cases non-negligible differences.

We also discuss the influence of the adopted initial mass function (IMF) on integrated colours and mass-to-light ratios and the effect of changing the maximum mass ($M_{\rm up}$) for which carbon burning is not ignited, due to effects by the degenerate pressure and neutrino energy losses in the core. The assumption of a fixed $M_V^{\rm tot}$ can lead to a peculiar behaviour when varying the shape of the IMF, since an adjustment of the total number of stars might be required to keep the $M_V^{\rm tot}$ value fixed.

The layout of the paper is the following. In Sect. 2 the ingredients of the stellar population synthesis code are outlined, including a brief description of the method adopted to derive the integrated quantities. In Sect. 3 we show the comparison of the theoretical results with selected observations of galactic globular clusters. Then, we discuss the uncertainties affecting integrated colours (Sect. 4) and mass-to-light ratios (Sect. 5), together with a comparison with previous works.

2. Description of the code

Synthetic CMDs and magnitudes presented in this paper are based on the stellar population synthesis code developed by Brocato et al. (1999, 2000) and Raimondo et al. (2005)[1]. In this section, we briefly describe the main ingredients and recall the method used to derive integrated magnitudes and colours, and refer the reader to the cited papers for more details.

2.1. Ingredients

The present SSP models rely on the evolutionary tracks of the "Pisa Evolutionary library"[2] for masses $M \geq 0.6\ M_\odot$ (Cariulo et al. 2004). The input physics adopted in the stellar evolution models has already been discussed in Cariulo et al. (2004). We only point out here that the models take atomic diffusion into account, including the effects of gravitational settling and thermal diffusion with diffusion coefficients given by Thoul et al. (1994); radiative acceleration (see e.g. Richer et al. 1998; Richard et al. 2002) is not included. The effects of rotation (see e.g. Maeder & Zahn 1998; Palacios et al. 2003) are also not included. Convective regions, identified following the Schwarzschild criterion, are treated with the mixing-length formalism. Moreover, the canonical assumption of inefficient overshooting is used, so the He-burning structures are calculated according to the prescriptions of canonical semiconvection induced by the penetration of convective elements in the radiative region (Castellani et al. 1985). The efficiency and presence of a mild overshooting are still open questions (Barmina et al. 2002; Brocato et al. 2003); however, as discussed in Yi (2003), a modest amount of overshooting (i.e. $H_P \sim 0.2$, see also Brocato et al. 2003) influences only integrated colours of those stellar populations with ages $\lesssim$1.5 Gyr for a maximum amount of $\approx$0.1 mag. Finally, the stellar models span the evolutionary phases from the main sequence up to C ignition or the onset of thermal pulses (TP) in the advanced asymptotic giant branch (AGB) in the mass range $0.6 \div 11\ M_\odot$. This allows us to calculate stellar population models in the age range $\approx$50 Myr $\div$ 20 Gyr.

Beyond the early-AGB phase, thermally pulsating (TP) stars are simulated in our synthesis code using the analytic formulas of Wagenhuber & Groenewegen (1998) which describes the time evolution of the core mass and luminosity of TP stars. These formulae include three important effects: (*i*) the first pulses do not reach the full amplitude, (*ii*) the hot bottom burning process that occurs in massive stars, and (*iii*) the third dredge-up. The effective temperature ($T_{\rm e}$) of each TP-AGB star is evaluated using prescriptions by Renzini & Voli (1981), considering the appropriate slope ${\rm dlog}(L/L_\odot)/{\rm dlog}(T_{\rm e})$ of the adopted evolutionary tracks. The analytic procedure ends up providing the time evolution of the temperature and luminosity for a given mass (see for details Raimondo et al. 2005).

Mass loss affecting red giant branch (RGB) stars and early-AGB stars is taken into account following prescriptions by Reimers (1975)

$$\dot{M}_{\rm R} = -4 \times 10^{-13} \eta_{\rm R} \cdot LR/M, \tag{1}$$

while during the TP phase we adopt the Baud & Habing (1983) mass-loss rate:

$$\dot{M}_{\rm BH} = \mu LR/M_{\rm e}. \tag{2}$$

Here, $L, R, M, M_{\rm e}$ are, respectively, the star luminosity, radius, total mass, and envelope mass in solar units; $\mu = -4 \times 10^{-13}(M_{\rm e,0}/M)$, being $M_{\rm e,0}$ the envelope mass at the first TP. Equation (2) is a modification of the Reimers formula with $\eta_{\rm R} = 1$, which also includes a dependence on the

[1] `http://www.oa-teramo.inaf.it/SPoT`

[2] `http://astro.df.unipi.it/SAA/PEL/Z0.html`. Data files are also available at the CDS.

actual mass envelope. The initial-final mass relation is from Dominguez et al. (1999), and no white dwarfs (WD) more massive than 1.1 $M_\odot$ are accepted (Prada Moroni & Straniero 2006).

In this paper the TP phase is included, but we do not adopt any separation between C-rich and O-rich TP-stars. All stars are oxygen-rich when they enter the AGB phase. Whether or not they become C-stars primarily depends on the efficiency of the third dredge-up (TDU) occurring in the TP-AGB phase and on the extent and time-variation of the mass loss (e.g. Marigo et al. 1999; Straniero et al. 2003). In low-metallicity stars ($Z < 0.004$), the amount of oxygen in the envelope is so low that a few thermal pulses are sufficient to convert an O-rich star into a C-star (Renzini & Voli 1981). In addition, the lower the metallicity the lower the minimum mass for the onset of TDU (e.g. Straniero et al. 2003). On the other hand, TP-AGB stars may experience episodes of strong mass loss, which in the case of low mass stars may cause a reduction of the envelope mass that may delay or even prevent the TDU occurrence and the formation of C-rich stars (Marigo et al. 1999).

In conclusion, the presence of C-rich stars may affect NIR-bands luminosity and its uncertainty in the case of low-metallicity, intermediate-age massive clusters (see e.g. Maraston 1998), while at the typical age of Galactic globular clusters their presence becomes more uncertain, as confirmed by the fact that AGB stars in GGC are all observed to be oxygen-rich, so that carbon does not appear to have been dredged up into the envelop during thermal pulses (Lattanzio & Wood 2003). Our assumption is also expected to have a marginal effect on integrated quantities of faint populations, as bright TP-AGB stars are statistically less frequent, or even absent. Finally, it will be shown that the details and the treatment of the physical processes at work in the TP-AGB phase, as well as their impact on synthetic colours, is still uncertain (Sect. 4).

The adopted colour transformations for the standard *UBVRIJHK* bands are from Castelli (1999), see also Castelli et al. (1997). To calculate integrated colours in the Hubble Space Telescope (HST) bands (WFPC2 and NICMOS systems), we adopt the colour transformations by Origlia & Leitherer (2000) based on the Bessell et al. (1998) stellar atmospheric models.

As is well-known, the mixing-length parameter (α) governs the efficiency of convection in the convective envelope of a stellar structure. In the evolutionary tracks of Cariulo et al. (2004) the α parameter has been calibrated in such a way that the isochrones reproduce, with the adopted colour transformations, the observed RG branch colour of GCs with the proper metallicity and age. This is evident from Fig. 2 in which our synthetic models nicely reproduce the RGB colours of the selected GCs. The α parameter needed to obtain this agreement is $\alpha \approx 2.0$, but it is worth noticing that α is a free parameter that is sensitive to the chosen colour transformations and on all the adopted physical inputs that affect the effective temperature of a model. Cariulo et al. (2004) show that tracks with the same physical assumptions for metallicity up to $Z \approx 0.001$ reproduces the RGB colours of galactic GCs for the same α values, while metal-rich ($Z > 0.001$) and standard solar models require a slightly lower α (see Ciacio et al. 1997; Castellani et al. 2003).

In this work the very low-mass tracks (VLM, $M \leq 0.6\ M_\odot$) are taken from Baraffe et al. (1997). The tracks have been already transformed by the authors to the observational plane in the Johnson-Cousins system after adopting the colour transformations by Allard et al. (1997), particularly suitable for low-mass stars. We checked that low-mass models satisfactorily match the higher mass models in all the available colours (Fagiolini 2004). However, as already discussed by e.g.

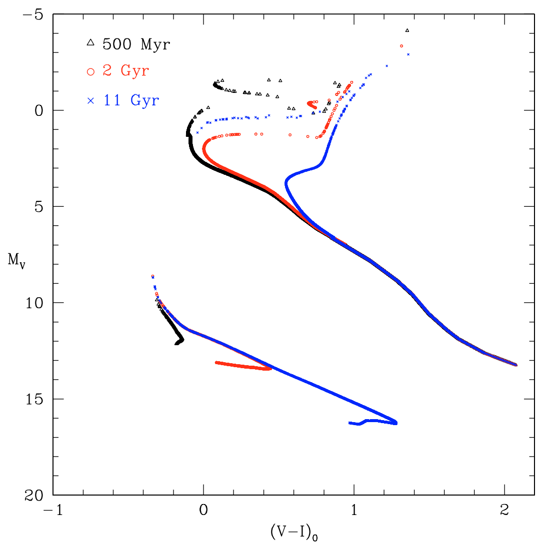

Fig. 1. Synthetic CMDs for $Z = 0.0002$, $Y = 0.23$, and three different ages: 500 Myr (black), 2 Gyr (red), and 11 Gyr (blue). For each population, $M_V^{\rm tot} = -6$ mag is adopted. The simulation of photometric errors is not included.

Brocato et al. (2000), VLM stars do not contribute to the photometric indices, although their contribution to the cluster mass is fundamental. Masses lower than the minimum mass for the central H ignition $M \approx 0.08\ M_\odot$ do not significantly contribute to the total mass of the cluster (see e.g. Chabrier & Mera 1997), and so they are not taken into account.

Post-AGB evolution experienced by stars before entering the white dwarfs (WD) cooling sequence is not considered because the evolutionary time is too short to have a significant influence (see e.g Bloecker & Schoenberner 1997). WDs are included in the code using evolutionary models by Salaris et al. (2000). The tracks have been transformed by the authors after adopting the atmospheric models by Saumon & Jacobson (1999) for DA WDs, which include the collision-induced absorption of H_2 molecules for $T < 4000$ K. For higher temperatures, the transformations of Bergeron et al. (1995) were used. Our *standard* model adopts $M_{\rm up} = 6.5\ M_\odot$ (Dominguez et al. 1999). As expected, and as already noted by e.g. Angeletti et al. (1980), the contribution of the WD population to optical and NIR photometric indices is negligible, although they contribute to the total mass of the cluster significantly.

The IMF of Kroupa (2002) is adopted in the mass interval $0.1 \leq M/M_\odot \leq 11$, unless explicitly stated otherwise. To simulate the mass distribution of stars in the synthetic CMD, we used a Monte Carlo method: the position of each randomly created star in the $\log L/L_\odot$ vs. $\log T_{\rm e}$ diagram was determined for each given age. As already discussed, the chemical composition is fixed to $Z = 0.0002$ and $Y = 0.23$.

Figure 1 shows, as an example, synthetic CMDs (without simulation of photometric errors) for the selected chemical composition, a total absolute visual magnitude $M_V^{\rm tot} = -6$ mag, and three different ages (500 Myr, 2 Gyr, and 11 Gyr). All the evolutionary phases described above are clearly visible.

2.2. Integrated magnitudes and colours

To compute integrated fluxes and magnitudes, we assume that the integrated light from the stellar population is dominated by light emitted by its stellar component. This implies that i) no source of non-thermal emission are at work, ii) the thermal emission by interstellar gas gives no sizeable contribution to the integrated flux, and iii) the absorption from dust and gas are negligible. On this basis, the integrated flux in each photometric filter mainly depend on two quantities. The first is the flux f_i emitted by the ith star of mass M, age t (stellar system age), luminosity l, effective temperature $T_{\rm eff}$, and chemical composition (Y, Z):

$$f_i[l(M,t,Y,Z), T_{\rm eff}(M,t,Y,Z), Y, Z] \quad (3)$$

here f_i is defined by the stellar evolutionary-tracks library and by the adopted temperature-colour transformation tables. The second quantity is $\Phi(M, N)$, which describes the number of stars with mass M in a population globally constituted of N stars with age t and chemical composition (Y, Z). It is strictly related to the IMF.

A fundamental point of our code is that the mass of each generated star is obtained by using Monte Carlo techniques, while the mass distribution is ruled by the IMF. The mass of each star is generated randomly, and its proper evolutionary line is computed by interpolating the available tracks in the mass grid. This method is crucial for poorly populated stellar systems, as we study in the following. It ensures that the undersampled evolutionary phases are treated properly; for instance, NIR colours may be dominated by a handful of red giant stars (Santos & Frogel 1997; Brocato et al. 1999; Cerviño & Valls-Gabaud 2003; Raimondo et al. 2005).

In each model, stars are added until reaching a given value of the absolute visual magnitude, M_V, at any age. The mass values are generated randomly and distributed according to the chosen IMF. It is relevant that the random extraction of masses is fully independent from model to model even if the same input quantities (M_V, t, N, Y, Z, IMF, etc.) are assumed.

Both the previous quantities (f_i and $\Phi(M, N)$) are combined and integrated by the stellar population code to derive the total integrated flux F in a given photometric band

$$F[N, t, Y, Z] = \sum_{i=1}^{N} f_i, \quad (4)$$

and the corresponding magnitudes.

3. Comparison with Galactic globular clusters

Before studying the general behaviour of colours and mass-to-light ratios as a function of M_V, the natural test for SSP models is to compare their predictions to the observed properties of Galactic star clusters. Three old galactic globular clusters (GGCs) were selected for checking our capability of reproducing both the CMD morphology of each cluster and the integrated magnitudes: NGC 4590 (M 68), NGC 7078 (M 15), and NGC 7099 (M 30). They are all metal-poor, span a relativity wide range of the visual magnitude (Table 1), and show different horizontal branch morphologies. This allows us to check the effect of HB morphologies on the integrated colours in the selected bands. The [Fe/H] values estimated for the three clusters are, respectively, [Fe/H] = –2.06, –2.26, –2.12 (Harris 1996)[3], while the α-elements enhancement can be evaluated as $[\alpha/{\rm Fe}] \approx 0.3$ (see, e.g., the discussion in Ferraro et al. 1999); thus we can assume $Z \approx 2 \times 10^{-4}$. We include M 15 due to its brightness ($M_V \sim -9$), even if it is recognised as a cluster that should have undergone a gravothermal catastrophe. This results in a contraction of the cluster core while the external regions expand, with some stars escaping the system. As a possible consequence of such a dynamical evolution, observational evidence of mass segregation and of radial color gradients has been found (Bailyn et al. 1989; De Marchi & Paresce 1994; Stetson & West 1994).

Figure 2 shows the observed CMDs for the selected clusters. The B and V photometry comes from the HST-Snapshot Catalog by Piotto et al. (2002), except for M 68 whose data are from Walker (1994). The synthetic CMD that better reproduces the observational data is over-plotted in each panel. An age of 11 Gyr is assumed for each cluster; we are not interested in a detailed calibration of the cluster ages, which is far from

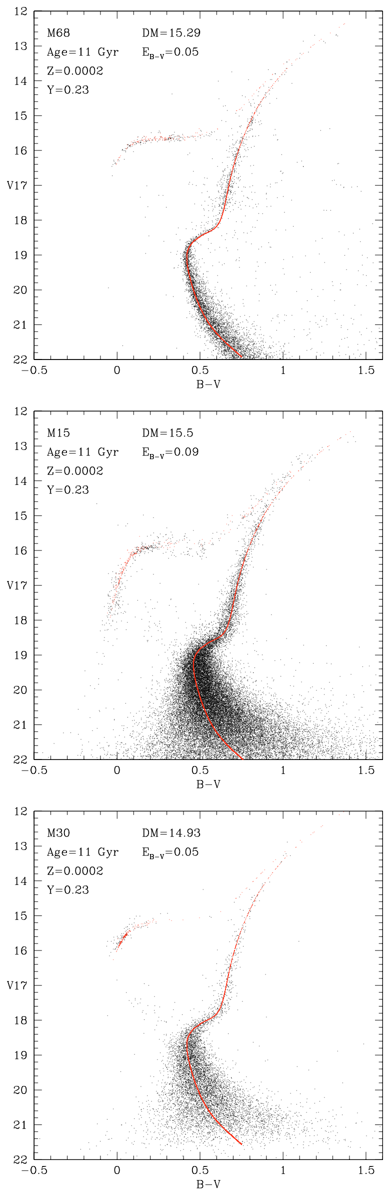

Fig. 2. Comparison between present synthetic CMDs (red dots), without the inclusion of simulated photometric errors, and the observed ones of the globular clusters *M 68*, *M 15*, and *M 30* (black dots). The assumed age is 11 Gyr, and the adopted chemical composition is $Z = 0.0002$ and $Y = 0.23$ (see text). The values of the distance modulus and the reddening obtained from the analysis are also indicated.

[3] www.physics.mcmaster.ca/resources/globular.html. February 2003 version.

Table 1. Observed and theoretical integrated colours for the selected globular clusters. Values from the Harris catalogue are dereddened according to Reed et al. (1988). The $J-K$ near-IR colour is from Brocato et al. (1990a), dereddened according to Cardelli et al. (1989). $\mathcal{M}/L_V$ is from the compilation by Pryor & Meylan (1993).

Identity	$M_V^{\rm tot}$	$U-B$	$B-V$	$V-R$	$V-I$	$J-K$	$\mathcal{M}/L_V$
Observations							
M 68	−7.35	−0.01 ± 0.01	0.58 ± 0.03	0.43	0.88 ± 0.01	–	1.6
M 15	−9.17	−0.03 ± 0.02	0.58 ± 0.01	–	0.73	0.62	2.2
M 30	−7.43	0.00 ± 0.02	0.57 ± 0.04	0.39 ± 0.02	0.82 ± 0.04	0.54	2.5
Models							
M 68	−7.34 ± 0.05	0.00 ± 0.02	0.60 ± 0.02	0.42 ± 0.01	0.87 ± 0.02	0.57 ± 0.07	1.79 ± 0.07
M 15	−9.18 ± 0.02	0.00 ± 0.01	0.60 ± 0.01	0.420 ± 0.003	0.89 ± 0.01	0.59 ± 0.02	1.58 ± 0.03
M 30	−7.43 ± 0.05	−0.01 ± 0.01	0.59 ± 0.02	0.41 ± 0.01	0.87 ± 0.02	0.54 ± 0.05	1.76 ± 0.07

our purpose. Results for each comparison between synthetic and observed cluster are, briefly:

– *M 68* (NGC 4590): We find $(m-M)_V = 15.29$ and $E_{B-V} = 0.05$ in agreement, within the uncertainties, with the current distance modulus and reddening determinations (e.g. Harris 1996; Carretta et al. 2000; Di Criscienzo et al. 2004). The HB morphology is reproduced using $\eta_R = 0.30$ with a dispersion $\sigma_\eta = 0.08$. Due to the present uncertainties in the factors that influence the HB morphology and in the precise treatment of mass loss in the RG branch (see e.g. Lee et al. 1994; Rey et al. 2001), the tuning of the adopted value of η_R is just a way to obtain the observed HB morphology, but it should not be interpreted in terms of the physical parameters of the stellar cluster.

– *M 15* (NGC 7078): The best fit is obtained by assuming $(m-M)_V = 15.50$ and $E_{B-V} = 0.09$, in agreement with current determinations of the cluster distance modulus and reddening (Harris 1996; Di Criscienzo et al. 2004; McNamara et al. 2004). The HB morphology is reproduced using $\eta_R = 0.44$ and $\sigma_\eta = 0.1$. The cluster contains one of the few planetary nebulae (PN) known in GGCs: the star K648 identified as a PN by Pease (1928), for which Alves et al. (2000) measured an apparent magnitude of $V = 14.73$.

– *M 30* (NGC 7099): Assuming $E_{B-V} = 0.05$, we obtain $(m-M)_V = 14.93$ in agreement with Sandquist et al. (1999). The HB morphology is reproduced using the same parameters as in Brocato et al. (2000), i.e. $\eta_R = 0.40$ and $\sigma_\eta = 0.2$.

Table 1 gives the observed integrated colours for the selected clusters, taken from the *Catalog of Parameters for Milky Way Globular Clusters* (Harris 1996)[4] and synthetic integrated colours obtained from the present models by reproducing, within the errors, the observed total visual magnitude of each cluster. Optical observational data are de-reddened according to Reed et al. (1988) with reddening values taken from Harris (1996). To give an idea of uncertainties for the colours, we report the "residual" values computed by Reed (1985) that result from his homogenization procedure based on measurements of cluster colours by various authors. In some cases the availability of only one measurement prevents the determination of an uncertainty. The NIR colours are from Brocato et al. (1990a), de-reddened according to Cardelli et al. (1989) with reddening values taken from Harris (1996).

Theoretical errors correspond to 1σ dispersion evaluated from 10 independent simulations. Table 1 lists: cluster identifier (Col. 1), total absolute V magnitude ($M_V^{\rm tot}$, Col. 2), integrated $U-B$, $B-V$, $V-R$, $V-I$, $V-J$, and $V-K$ colours (Cols. 3–7), and $\mathcal{M}/L_V$ (Col. 8) from Pryor & Meylan (1993). The last values are strongly model-dependent, as stressed by the authors themselves. Hereinafter we indicate dereddened colours such as, e.g., $U-B$ instead of $(U-B)_0$.

For each cluster, numerical simulations were performed by populating the synthetic CMD until the observed $M_V^{\rm tot}$ of the cluster is reproduced (Sect. 2.1). Synthetic colours agree with data of all the clusters to within the uncertainties and theoretical statistical fluctuations. The only exception is the $V-I$ colour of M 15 that is found to be redder than observations. The observed $V-I$ colour of this cluster is significantly bluer than that of other clusters with similar metallicity (Harris 1996). In this regard, we recall that the available $V-I$ measure is based only on one photoelectric measurement (Kron & Mayall 1960), and it is not possible to estimate the uncertainty (Reed 1985). To investigate this issue, we used VI stellar photometry by Rosenberg et al. (2000), which contains more than 90% of the cluster light ($M_V \simeq -9.1$). By adding the flux of individual stars, we derived an integrated colour $V-I \simeq 0.85$, in fair agreement with our prediction. This value is higher than the integrated value by Kron & Mayall (1960), even if it might be affected by incompleteness at the faint end of the observed luminosity function. To investigate the origin of the latter inconsistency in detail is well beyond the purpose of this paper, but what we wish to point out here is that the observed integrated $V-I$ colour of such a cluster, reported in Table 1, could be peculiar and hence not representative of metal-poor clusters.

Additional indications may come from analysing the M 15 NIR colours. The $J-K$ prediction agrees well with the value by Brocato et al. (1990a, $J-K = 0.67$, reddened) and is also consistent with data by Burstein et al. (1984), who found $J-K = 0.62$ (reddened). Interestingly, Burstein et al. (1984) also provide the observed $(V-K) = 2.14$ (reddened), which becomes $(V-K) = 1.86$ if corrected according to our reddening assumptions. By comparing this value with theory ($V-K = 2.05$), it appears that our models predict a $V-K$ colour about 0.2 mag redder than observations. Unfortunately, a similar comparison cannot be made for M 30 and M 68, since they are not listed by Burstein et al. (1984). Instead, the authors observed M 92 (NGC 6341), whose metallicity is estimated to be close to M 15, being [Fe/H] = −2.29. Since M 92 is as bright as $M_V = -8.20$, its colours data can be easily compared with our predictions, as reported in Table 2, at age ∼11–13 Gyr. Interestingly, the observed optical-NIR colour $V-K = 2.13$ agrees well with our prediction, together with all the optical colours $U-B = 0.01$, $B-V = 0.61$, and $V-I = 0.86$ (from Harris's catalog).

[4] `www.physics.mcmaster.ca/resources/globular.html`. February 2003 version. The integrated colours $U-B$ and $B-V$ are on the standard Johnson system, and $V-R$, $V-I$ on the Kron-Cousins system. The values are the simply average of results from Peterson (1993) and Reed (1985).

Table 2. Integrated colours in the *standard UBVRIJHK* photometric filters for our *standard* model with $M_V^{\rm tot} = -8$ and $Z = 0.0002$. (Full version available at CDS.)

Age (Myr)	$M_V^{\rm tot}$	$U-B$	$B-V$	$V-R$	$V-I$	$V-J$	$V-K$
50.	−8.0 ± 0.1	−0.56 ± 0.03	−0.10 ± 0.08	−0.02 ± 0.08	0.0 ± 0.2	0.0 ± 0.3	0.1 ± 0.5
100.	−8.0 ± 0.1	−0.39 ± 0.03	0.00 ± 0.07	0.06 ± 0.07	0.2 ± 0.2	0.4 ± 0.3	0.7 ± 0.5
150.	−8.0 ± 0.1	−0.31 ± 0.02	0.01 ± 0.04	0.06 ± 0.04	0.2 ± 0.1	0.4 ± 0.2	0.7 ± 0.3
200.	−8.00 ± 0.05	−0.22 ± 0.01	0.09 ± 0.05	0.14 ± 0.05	0.4 ± 0.1	0.7 ± 0.2	1.2 ± 0.3
300.	−8.01 ± 0.09	−0.12 ± 0.02	0.14 ± 0.07	0.16 ± 0.07	0.4 ± 0.1	0.8 ± 0.2	1.3 ± 0.4
400.	−8.06 ± 0.08	−0.05 ± 0.01	0.16 ± 0.04	0.16 ± 0.04	0.41 ± 0.09	0.8 ± 0.2	1.3 ± 0.2
500.	−8.02 ± 0.05	−0.01 ± 0.01	0.19 ± 0.03	0.18 ± 0.03	0.44 ± 0.07	0.8 ± 0.1	1.3 ± 0.2
600.	−8.06 ± 0.08	0.00 ± 0.01	0.26 ± 0.03	0.22 ± 0.03	0.52 ± 0.06	1.0 ± 0.1	1.4 ± 0.2
800.	−8.03 ± 0.06	0.01 ± 0.01	0.34 ± 0.04	0.27 ± 0.03	0.62 ± 0.07	1.1 ± 0.1	1.7 ± 0.2
1000.	−7.98 ± 0.04	0.00 ± 0.01	0.36 ± 0.02	0.28 ± 0.01	0.63 ± 0.03	1.13 ± 0.06	1.6 ± 0.1
1100.	−8.02 ± 0.06	0.00 ± 0.01	0.39 ± 0.03	0.30 ± 0.02	0.66 ± 0.04	1.16 ± 0.07	1.68 ± 0.09
1500.	−8.03 ± 0.04	0.01 ± 0.01	0.41 ± 0.02	0.30 ± 0.01	0.67 ± 0.02	1.17 ± 0.04	1.70 ± 0.07
1700.	−8.00 ± 0.04	0.02 ± 0.01	0.42 ± 0.02	0.31 ± 0.01	0.68 ± 0.03	1.20 ± 0.06	1.73 ± 0.08
2000.	−7.97 ± 0.03	0.03 ± 0.01	0.44 ± 0.01	0.32 ± 0.01	0.71 ± 0.02	1.24 ± 0.04	1.78 ± 0.05
3000.	−7.98 ± 0.05	0.03 ± 0.01	0.49 ± 0.02	0.35 ± 0.01	0.75 ± 0.02	1.29 ± 0.03	1.83 ± 0.05
4000.	−8.04 ± 0.06	0.01 ± 0.01	0.53 ± 0.02	0.37 ± 0.01	0.79 ± 0.02	1.34 ± 0.03	1.89 ± 0.05
5000.	−8.01 ± 0.05	0.00 ± 0.01	0.55 ± 0.02	0.38 ± 0.01	0.80 ± 0.02	1.35 ± 0.04	1.89 ± 0.05
6000.	−8.02 ± 0.03	−0.02 ± 0.01	0.57 ± 0.01	0.39 ± 0.01	0.83 ± 0.01	1.39 ± 0.02	1.94 ± 0.03
7000.	−8.03 ± 0.04	−0.02 ± 0.01	0.60 ± 0.01	0.41 ± 0.01	0.85 ± 0.01	1.43 ± 0.02	1.99 ± 0.03
8000.	−8.00 ± 0.03	−0.02 ± 0.01	0.61 ± 0.01	0.41 ± 0.01	0.86 ± 0.01	1.44 ± 0.02	2.00 ± 0.03
9000.	−7.99 ± 0.02	−0.01 ± 0.01	0.61 ± 0.01	0.41 ± 0.01	0.87 ± 0.01	1.45 ± 0.02	2.02 ± 0.02
10000.	−7.94 ± 0.03	−0.00 ± 0.01	0.61 ± 0.01	0.42 ± 0.01	0.87 ± 0.01	1.47 ± 0.02	2.04 ± 0.03
11000.	−8.01 ± 0.04	0.00 ± 0.01	0.60 ± 0.01	0.42 ± 0.01	0.87 ± 0.01	1.46 ± 0.02	2.04 ± 0.02
12000.	−7.99 ± 0.04	0.00 ± 0.01	0.61 ± 0.01	0.42 ± 0.01	0.88 ± 0.01	1.48 ± 0.02	2.06 ± 0.03
13000.	−7.95 ± 0.05	0.01 ± 0.01	0.62 ± 0.02	0.43 ± 0.01	0.90 ± 0.02	1.51 ± 0.03	2.10 ± 0.04
14000.	−8.00 ± 0.04	0.00 ± 0.01	0.63 ± 0.01	0.43 ± 0.01	0.90 ± 0.01	1.52 ± 0.02	2.11 ± 0.03
15000.	−8.01 ± 0.04	−0.02 ± 0.01	0.62 ± 0.02	0.43 ± 0.01	0.90 ± 0.01	1.51 ± 0.03	2.10 ± 0.04

In conclusion, except for the peculiarity concerning M 15, our models are able to properly predict the integrated colours of, let us say, "normal" metal-poor clusters, as confirmed by the comparison with the observational data of M 30, M 68 (Table 1), and the additional cluster M 92.

As noted above, $\mathcal{M}/L$ values reported in the last column of Table 1 (upper section), derived using isotropic King models by Pryor & Meylan (1993), are strongly model-dependent, and thus the reported values are only indicative. Moreover, dynamical processes, such as star evaporation (e.g. Spitzer 1987; Vesperini & Heggie 1997), may affect the total mass and the inferred IMF shape as a function of time. Observed integrated colours of the selected clusters, as well as theoretical results, indicate that they are not influenced by the HB morphology, at least in our modeled photometric bands. Shorter wavelength ultraviolet colours are expected to be more sensitive to the presence of an extended blue HB.

4. Integrated colours

In this section we examine the effects on integrated colours of stochastic fluctuations for different values of the assumed total absolute visual-magnitude and the effects of the still present uncertainty on the IMF shape. The Kroupa (2002) IMF is adopted for the *standard* model.

Results are presented at fixed absolute visual-magnitude to aid comparisons with observational data. For these calculations the evaluation of the statistical fluctuations is fundamental. Statistical fluctuations of broad-band colours, as well as mass-to-light ratios, were evaluated by computing a series of 10 independent simulations for a fixed set of population's parameters (Z, age, IMF, ...) at fixed $M_V^{\rm tot}$, and by assuming a 1σ error. When fluctuations become large, and the value above is not fully representative of colours variations, we extend the analysis up to 100 runs. This is especially the case of very poorly populated clusters ($M_V = -4$) and young ages.

The *standard* models are computed assuming: $\eta_R = 0.3$, $\sigma_\eta = 0.08$ and Kroupa's IMF. As an example, Tables 2 and 3 report integrated colours as a function of age for models with $M_V^{\rm tot} = -8$; Johnson-Cousins colours in Table 2 and HST colours in Table 3. Table 2 lists from left to right: age, $M_V^{\rm tot}$, integrated $(U-B)$, $(B-V)$, $(V-R)$, $(V-I)$,$(V-J)$, and $(V-K)$ colours. Table 3 reports from left to right: age, $V-F439W2$, $V-F555W2$, $V-F814W2$ for the $WFPC2$ and $V-F110W1$, $V-F160W1$ for the $NICMOS$ camera.

4.1. $M_V^{\rm tot}$ sensitivity

Our standard synthetic models are calculated for three different values of the total magnitude: $M_V^{\rm tot} = -8, -6$, and -4 (all the results for both broad-band colours and mass-to-light ratios for $M_V^{\rm tot} = -6$ and -4 models are available as electronic tables at the CDS).

In Fig. 3 the time evolution of selected integrated colours is shown for the two extreme cases ($M_V^{\rm tot} = -8$ and -4). In general, broad-band colours become redder with age, because of the increasing fraction of cool stars in the populations. For the same reason, the $(U-B)$ colour is quite age-insensitive for age $\gtrsim$1 Gyr.

Within the statistical uncertainties, the mean colours at different $M_V^{\rm tot}$ do not show significant differences, except in a few cases at young ages and for optical-NIR colours. This is due to the strong variation in the number of very bright red stars significantly affecting the total luminosity of the cluster. In an SSP with a total brightness as faint as $M_V^{\rm tot} = -4$, most of the stars occupy the MS phase, and only a few (or none) red giants are present, including stars burning He in the core and stars in the double-shell

Table 3. As in Table 2 but for WFPC2 (first three columns) and NICMOS1 (last two columns) photometric bands. (Full version available at CDS.)

Age (Myr)	$V - 439W(2)$	$V - F555W(2)$	$V - F814W(2)$	$V - F110W(1)$	$V - F160W(1)$
50.	0.09 ± 0.08	0.009 ± 0.005	0.0 ± 0.2	0.0 ± 0.3	0.0 ± 0.5
100.	−0.01 ± 0.08	0.002 ± 0.005	0.2 ± 0.2	0.3 ± 0.3	0.6 ± 0.5
150.	−0.02 ± 0.03	0.000 ± 0.002	0.2 ± 0.1	0.3 ± 0.1	0.6 ± 0.3
200.	−0.11 ± 0.05	−0.006 ± 0.003	0.3 ± 0.1	0.6 ± 0.2	1.1 ± 0.3
300.	−0.15 ± 0.07	−0.009 ± 0.004	0.4 ± 0.1	0.6 ± 0.2	1.2 ± 0.4
400.	−0.18 ± 0.05	−0.011 ± 0.003	0.4 ± 0.09	0.6 ± 0.1	1.2 ± 0.2
500.	−0.21 ± 0.04	−0.013 ± 0.002	0.42 ± 0.07	0.7 ± 0.1	1.2 ± 0.2
600.	−0.28 ± 0.04	−0.018 ± 0.002	0.50 ± 0.06	0.8 ± 0.1	1.3 ± 0.1
800.	−0.38 ± 0.04	−0.023 ± 0.002	0.60 ± 0.07	0.9 ± 0.1	1.5 ± 0.1
1000.	−0.40 ± 0.02	−0.024 ± 0.001	0.61 ± 0.03	0.93 ± 0.05	1.53 ± 0.08
1100.	−0.43 ± 0.03	−0.025 ± 0.001	0.63 ± 0.04	0.99 ± 0.06	1.57 ± 0.10
1500.	−0.45 ± 0.02	−0.026 ± 0.001	0.64 ± 0.02	0.97 ± 0.04	1.58 ± 0.06
1700.	−0.46 ± 0.02	−0.027 ± 0.001	0.66 ± 0.03	0.99 ± 0.05	1.61 ± 0.08
2000.	−0.49 ± 0.01	−0.028 ± 0.001	0.68 ± 0.02	1.03 ± 0.03	1.66 ± 0.05
3000.	−0.55 ± 0.02	−0.031 ± 0.001	0.72 ± 0.02	1.07 ± 0.03	1.71 ± 0.05
4000.	−0.60 ± 0.02	−0.033 ± 0.001	0.76 ± 0.02	1.12 ± 0.03	1.77 ± 0.04
5000.	−0.61 ± 0.02	−0.033 ± 0.001	0.76 ± 0.02	1.11 ± 0.03	1.75 ± 0.04
6000.	−0.65 ± 0.01	−0.035 ± 0.001	0.89 ± 0.01	1.17 ± 0.02	1.82 ± 0.02
7000.	−0.67 ± 0.02	−0.035 ± 0.001	0.81 ± 0.02	1.18 ± 0.03	1.84 ± 0.04
8000.	−0.69 ± 0.01	−0.036 ± 0.001	0.83 ± 0.01	1.21 ± 0.02	1.88 ± 0.03
9000.	−0.70 ± 0.02	−0.036 ± 0.001	0.83 ± 0.01	1.22 ± 0.02	1.90 ± 0.03
10000.	−0.70 ± 0.01	−0.036 ± 0.001	0.84 ± 0.01	1.23 ± 0.02	1.92 ± 0.03
11000.	−0.69 ± 0.01	−0.035 ± 0.001	0.84 ± 0.02	1.23 ± 0.01	1.91 ± 0.02
12000.	−0.69 ± 0.01	−0.035 ± 0.001	0.85 ± 0.01	1.25 ± 0.02	1.94 ± 0.03
13000.	−0.71 ± 0.02	−0.036 ± 0.001	0.86 ± 0.01	1.27 ± 0.02	1.97 ± 0.03
14000.	−0.72 ± 0.01	−0.036 ± 0.001	0.87 ± 0.01	1.28 ± 0.02	1.98 ± 0.03
15000.	−0.72 ± 0.02	−0.036 ± 0.001	0.87 ± 0.02	1.28 ± 0.02	1.97 ± 0.04

phase (see for example Fig. 14 in Raimondo et al. 2005). Hence, the mean $V - K$ colour (and to a lesser extent $V - I$) is generally bluer than in models with $M_V^{\rm tot} = -8$, where the post-MS phase is always widely populated. This effect is large in young clusters, for which colours are more sensitive to the cluster luminosity, see also Fig. 5 in Santos & Frogel (1997), and Fig. 8 in Brocato et al. (1999)[5].

To clarify this point, Fig. 4 illustrates the $V - K$ colour distribution for an SSP model with age 100 Myr and for each choice on $M_V^{\rm tot}$. The $V - K$ colour distribution of faint clusters shows a populous blue peak, due to the large fraction of simulations containing mainly *blue* stars, and a few sparse simulations at redder colours containing a few red giants. Consequently, the average colour is bluer than found for brighter clusters (Fig. 3), which show a broadened colour distribution shifted towards the red side, since the probability of having a large number of red stars is higher. We emphasise that, in the present paper, for a given cluster age the integrated colours at different cluster brightnesses are obtained by properly adding stars in all evolutionary phases according to the IMF and evolutionary time-scales (i.e. keeping the proportion between the number of stars in different stages fixed). By decreasing their absolute magnitude (mass), the *natural* trend is that the cluster progressively misses post-MS stars. In other words, due to the discreteness of stars "*if an SSP is far less luminous, then there would be no post-MS stars and the integrated fluxes would be dominated by upper MS stars with little spread in color, which results in smaller color fluctuations*" (Santos & Frogel 1997). The colour behaviour described above is in agreement with Santos & Frogel (1997) and Brocato et al. (1999), while opposite to what was found by Bruzual & Charlot (2003). A discussion of the nature of such a discrepancy is beyond the purpose of this paper, since it would require a detailed comparison between all the assumptions adopted in all the codes (evolutionary tracks, atmospheres, etc.).

In general, for a further increase in the cluster brightness, the stochastic effects decrease, the colour distribution becomes more regular, and the standard deviation decreases (small spread in colour).

At a given age, the size of errorbars increases as the cluster luminosity decreases, due to the small number of stars present in faint clusters ($M_V^{\rm tot} = -4$) with respect to bright ones ($M_V^{\rm tot} = -8$). From the figure it is evident that the statistical errors at $M_V^{\rm tot} = -4$ are high enough to prevent a precise evaluation of the age of the cluster.

The errorbars also increase from $B - V$ to $V - K$, as shown by Brocato et al. (1999). This last finding is related to the expected small number of post-MS stars shining in the infrared wavelengths, especially in the case of low-luminosity clusters ($M_V^{\rm tot} = -4$). Moreover, in faint clusters it may happen that giant stars are not present in each of the simulations we computed at a fixed age, since their appearance is highly driven by stochastic phenomena. At a fixed total magnitude, the *intrinsic* uncertainty lessens with age, also because a larger number of stars is needed to reach the given total magnitude.

4.2. IMF variations

To evaluate the effect of IMF variations on integrated colours, we changed the Kroupa (2002) IMF exponent (α) within the estimated uncertainty for masses $M > 0.5\,M_\odot$. In Fig. 5 models with $M_V^{\rm tot} = -8$ calculated with the lower, central, and upper values of the IMF exponent are plotted in selected pass-bands; the corresponding data tables are available as electronic tables at the CDS.

As obtained for metal-rich models investigated in previous papers (see e.g. Maraston 1998; Brocato et al. 2000; Yi 2003;

[5] We also refer the reader to the recent work by Cerviño & Luridiana (2004).

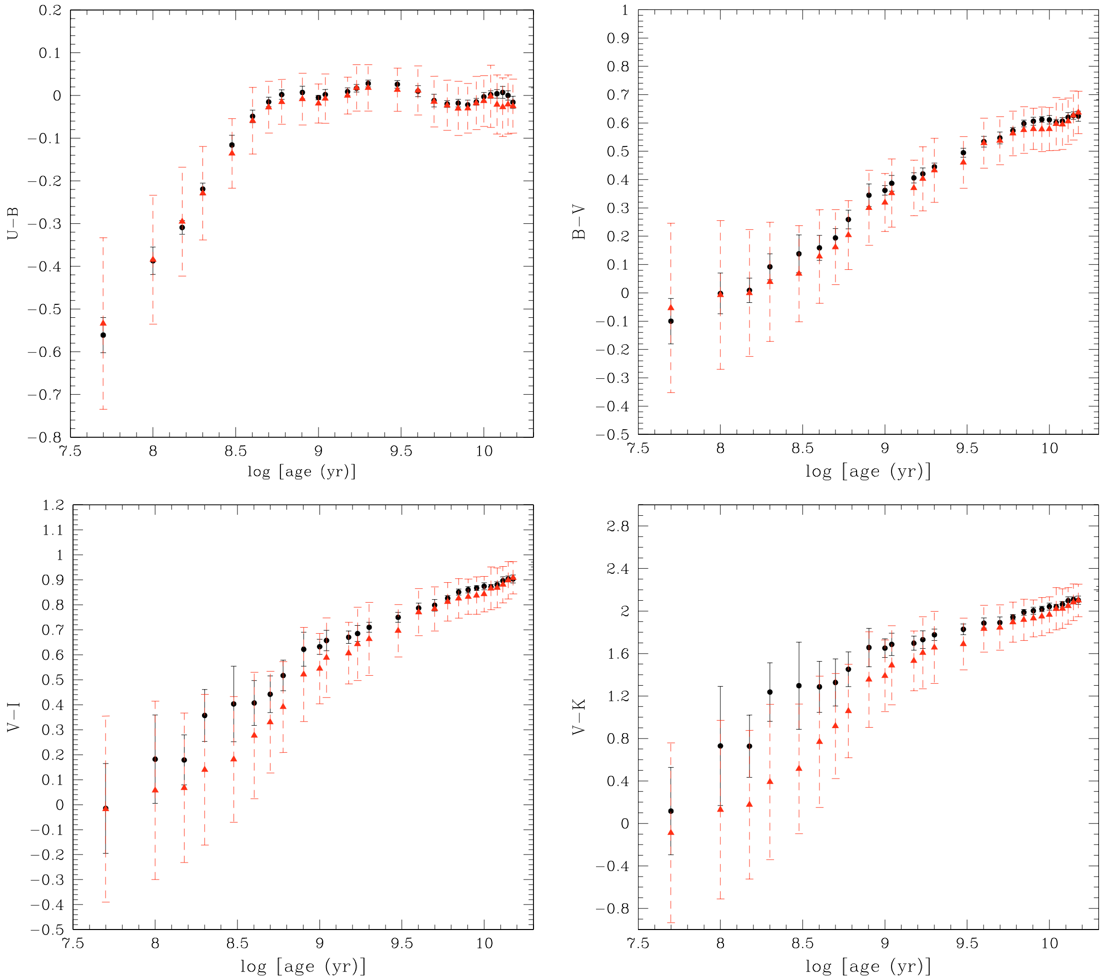

Fig. 3. Time evolution of selected integrated colours in the standard *UBVRIJHK* filters for models with $M_V^{\rm tot} = -4$ (red triangles, dashed lines) and $M_V^{\rm tot} = -8$ (black points, solid lines). 1σ colour dispersion is reported for each model, see text.

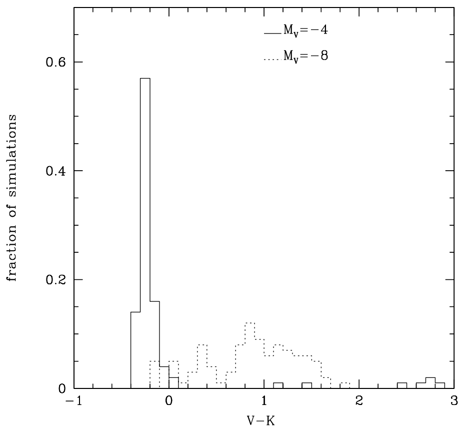

Fig. 4. $V - K$ colour distribution resulting from 100 simulations for a model with 100 Myr, $Z = 0.0002$, and $M_V^{\rm tot} = -4$ (solid) and -8 mag (dotted).

Bruzual & Charlot 2003), we find that colour variations are also negligible for very low-metallicity models, at least in the range of exponents investigated here, being the colour variations well within the intrinsic uncertainty, for both values of the brightness of the cluster ($M_V^{\rm tot} = -4$ mag and -8 mag). The errorbars behavior is similar to what described above: colour fluctuations increase from the optical-optical to optical-NIR colours and for ages $\lesssim$1 Gyr.

Changing the distribution of very low-mass stars ($M \leq 0.5\,M_\odot$) has negligible effects on photometric indices whatever the total visual magnitude, as already shown by Brocato et al. (2000) for ages greater than 5 Gyr. In poorly populated clusters as much as in the richest ones, reducing the number of stars with $M < 0.5\,M_\odot$ does not affect the integrated colours since the contribution of these stars to the total V light is only of the order of a few percent (Brocato et al. 2000). The contribution of such stars slightly increases with age, but it remains comparable to the statistical errors even at the oldest ages (at least in the range explored here).

4.3. Comparison with previous works

Table 4 summarises the main ingredients used by various authors in their synthesis code, and Fig. 6 compares the time-evolution of $B - V$ and $V - K$ colours of the present work with similar recent results available in the literature. In the figure our models are plotted with 1σ intrinsic error, while other authors do not estimate the colours' statistical errors, except for Brocato et al. (2000). If colours are not available for exactly the same metallicity value adopted in the present work ($Z = 0.0002$), the two closest Z values are plotted. In Fig. 6 we plot an updated version of the models of Anders & Fritze-v. Alvensleben (2003)[6].

[6] Models are updated concerning line emission (Anders, private communication).

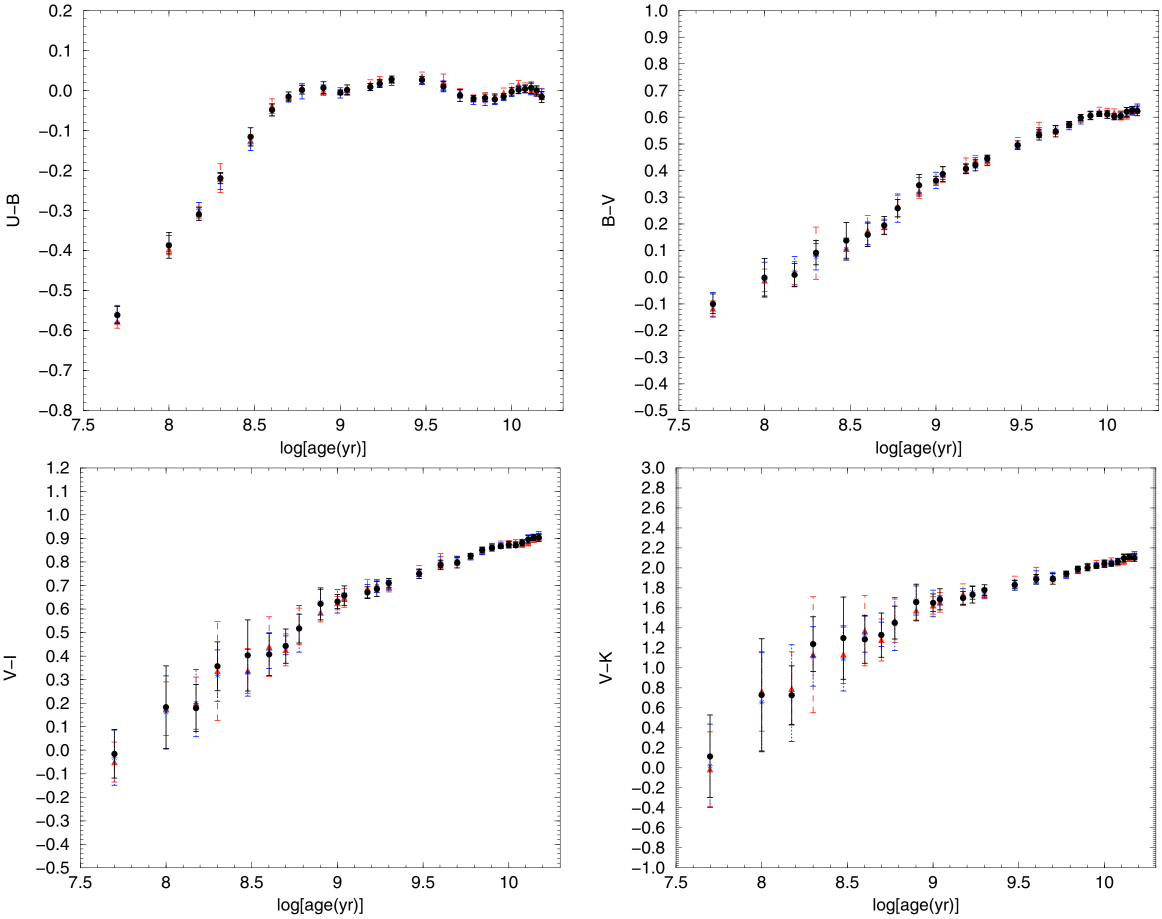

Fig. 5. Time evolution of selected integrated colours for SSPs with $M_V^{\rm tot} = -8$ calculated with the lower, central, and upper values for the Kroupa (2002) IMF exponent (α) for $M \geq 0.5\ M_\odot$. Black dots indicate our reference model ($\alpha = 2.3$), red triangles indicate models with $\alpha = 2.0$, and blue stars models with $\alpha = 2.6$.

The present predictions agree well with those by Brocato et al. (2000). There is also good agreement with Kurth et al. (1999) and Bruzual & Charlot (2003), both based on *Padua 1994* stellar evolutionary tracks (see the quoted papers for the detailed list of references). Differences can be found in the age range $8.6 \lesssim \log \mathrm{age(yr)} \lesssim 9$ for optical-NIR colours, possibly due to the treatment of the AGB and TP-AGB phases. Girardi et al. (2000) and Anders & Fritze-v. Alvensleben (2003) predict redder colours than all the other authors for age $\gtrsim$ 100 Myr, as do Zhang et al. (2002) for age $\gtrsim$ 3 Gyr. In contrast the others, both Maraston (2005) and our models are based on no-overshooting tracks. Nevertheless, while the present $B-V$ colours agree well with Maraston's models at all the ages in common, $V-K$ predictions are bluer than those by Maraston (2005) at ages younger than $\simeq$3 Gyr.

Figure 6 shows that the $B-V$ and $V-K$ predictions from different authors agree within 0.1 mag at $\log \mathrm{age} \gtrsim 9.3$. Large model-to-model differences arise at young and intermediate ages, when the contribution of AGB and TP-AGB stars to the total flux is high, especially in the NIR bands (see for a discussion Maraston 1998; Girardi & Bertelli 1998). This has a direct consequence on predicted colours, since a wide variety of stellar ingredients and prescriptions are used to simulate these phases. Temperature-colour relations, mass-loss prescriptions, and the analytical description of the TP evolution all affect the photometric properties of such stars, so that it is not straightforward to individuate a single origin (or multiple ones) to explain the differences shown in Fig. 6 in the intermediate-age range.

For instance, mass-loss processes are one of the physical mechanisms largely affecting the evolution of a TP-AGB star. However, the effect of mass loss on the observational properties of TP stars is largely unknown to date. To give an indication of how mass loss may affect colour predictions, we made numerical experiments by computing integrated colours in the extreme case when no TP-AGB stars are present in the population, thus mimicking a very efficient mass-loss rate (see also Maraston 1998). As expected, the effect is greater for intermediate-age populations and in the optical-NIR colours. The $V-K$ colour becomes bluer than the *standard* value by ~0.5 mag at age = 500 Myr, and the $B-V$ colour decreases only by 0.06 mag at the same age. This effect tends to vanish by increasing the age. On the other hand, if we lower the mass-loss efficiency with respect to our *standard* assumption (BH) by using a Reimers' law with η of the order of 1, and $V-K$ colours redder than our "standard" models are obtained. As a consequence the colour decline at an age corresponding to the appearance of He-core degenerate stars is more evident ($t \sim 1$ Gyr), similar to what is obtained by Maraston (2005) for integrated colours and by Raimondo et al. (2005) for surface brightness fluctuation colours.

5. Mass-to-light ratio

Table 6 lists our predictions for the mass-to-light ratio ($\mathcal{M}/L$) in various photometric bands as a function of age for $M_V^{\rm tot} = -8$; similar tables for $M_V^{\rm tot} = -6$ and $M_V^{\rm tot} = -4$ are available at the CDS.

Table 4. The physical ingredients adopted in the models plotted in Fig. 6.

Authors	Evolutionary tracks[a]	Stellar spectral library	IMF
Kurth et al. (1999)	Padua Lib. 1994 + Chabrier & Baraffe (1997)	Lejeune et al. (1997, 1998)	Salpeter (1955)
Brocato et al. (2000)	Frascati Lib. 1991-2000	Castelli et al. (1997)	Scalo (1986)
Girardi et al. (2000)	Padua Lib. 1994-2000	Kurucz (1992)	Salpeter (1955)
Zhang et al. (2002)	Pols et al. (1998)	Lejeune et al. (1997, 1998)	Kroupa et al. (1993)
Anders & Fritze-v. Alvensleben (2003)	Padua Lib. 1994-2000 + Chabrier & Baraffe (1997)	Lejeune et al. (1997, 1998)	Salpeter (1955)
Bruzual & Charlot (2003)	Padua Lib. 1994 + Baraffe et al. (1998)	Westera et al. (2002)	Chabrier (2003)
Maraston (2005)	Cassisi et al. (2000)	Lejeune et al. (1998)[b]	Kroupa (2001)[c]
Present work	Pisa Lib. 2004 + Baraffe et al. (1997)	Castelli (1999)	Kroupa (2002)

Authors	Normalization	Thermal Pulses	OS[d]	$M_{\rm up}$	WD[e]	$\mathcal{M}/L$[f]
Kurth et al. (1999)	–[g]	No	≈0.2	5	No	No
Brocato et al. (2000)	Number of stars & $M_V^{\rm tot}$	Groenewegen & de Jong (1993)	No	5	Yes	No
Girardi et al. (2000)	1 $M_\odot$	Groenewegen & de Jong (1993) + Marigo (1998)	≈0.25	5	Yes	No
Zhang et al. (2002)	1 $M_\odot$	Vassiliadis & Wood (1993)	0.22 ÷ 0.4	5	Yes	No
Anders & Fritze-v. Alvensleben (2003)	Initial cluster mass[h]	Groenewegen & de Jong (1993)	≈0.25	–[h]	Yes	Yes
Bruzual & Charlot (2003)	1 $M_\odot$	Vassiliadis & Wood (1993)[i]	≈0.2	5	Yes	Yes
Maraston (2005)	1 $M_\odot$	Renzini (1992)[i,j]	No	8.5	Yes	Yes
Present work	$M_V^{\rm tot}$	Wagenhuber & Groenewegen (1998)	No	6.5	Yes	Yes

[a] Detailed information on the adopted evolutionary tracks can be found in the paper quoted in Col. 1.
[b] The latest version available on the web, see Maraston (2005).
[c] Synthetic models are also calculated for the IMF of Salpeter (1955).
[d] The quoted values for the overshooting (OS) efficiency, expressed in units of pressure-scale-height above the Schwarzschild convective border, are only indicative because different sets of evolutionary tracks adopt different prescriptions for the overshooting mechanisms and for the minimum mass at which the overshooting is fully efficient (see the related papers for more details);
[e] This column indicates if WDs are included in the calculations.
[f] This column indicates if mass-to-light ratio values are available.
[g] In the paper by Kurth et al. (1999) the normalization procedure is not described.
[h] In the paper by Anders & Fritze-v. Alvensleben (2003) the SSPs have been evolved to the selected ages starting with an initial stellar mass of 10^6 $M_\odot$; the adopted value for $M_{\rm up}$ is not specified.
[i] Carbon stars are included.
[j] See discussion in Maraston (2005).

The total mass $\mathcal{M}$ includes all the evolving stars up to the AGB tip ($M \geq 0.1\,M_\odot$) and WDs. Stars with mass higher than $M_{\rm up} = 7\,M_\odot$ are assumed to leave a neutron star (NS) as a remnant. To evaluate the maximum mass fraction of NS, we set the neutron star mass at its upper limit (≈2 $M_\odot$, see e.g. Bombaci et al. 2004), and we chose high cluster age (≈12 Gyr); we found that the NS mass fraction constitutes at most a few percent of the cluster mass, in agreement with the calculations by Vesperini & Heggie (1997) who found an upper value of ≈1%. The contribution of massive black holes to the total mass depends on the assumption on the mass of the remnant and IMF (Maraston 2005). By using the same prescriptions on the black hole mass as Maraston (2005), we estimated that for a Kroupa IMF the mass fraction of both neutron stars and black holes does not exceed 5−10%.

In this paper, the $\mathcal{M}/L$ values are calculated without taking any dynamical processes into account, e.g. evaporation of stars due to two-body relaxation or disk shocking (see e.g. Spitzer 1987; Vesperini & Heggie 1997; Boily et al. 2005). A treatment of these phenomena is beyond the scope of this work; N-body simulations showing the effects of these processes on the total mass and IMF shape as a function of time and on the galactocentric distance of the cluster can be found in e.g. Vesperini & Heggie (1997). We only note that, since stellar evaporation is more efficient for low mass stars, one expects a flattening of the IMF as the dynamical evolution of a cluster proceeds. Evaluations of the mass fraction of WDs expected to be lost from clusters due to dynamical evaporation can be found in Vesperini & Heggie (1997) (see also Fellhauer et al. 2003; Hurley & Shara 2003). The presence of binary stars is not taken into account either; the lack of information about the binary frequency, the distribution of binaries of different mass ratios, the separation of the components, and the occurrence of explosions of novae and supernovae prevents a quantitative treatment of this phenomenon. An attempt to include binary systems in population synthesis models has recently been presented by Zhang et al. (2005).

In Fig. 7 we show the influence of VLM stars ($M \leq 0.6\,M_\odot$) and WDs on the $\mathcal{M}/L$, where L is the bolometric luminosity in solar units, at a fixed absolute visual magnitude ($M_V = -8$). As already known, VLM and WDs provide a nearly negligible contribution to the total luminosity (see for example Maraston 1998), while contributing significantly to the total mass. Figure 7

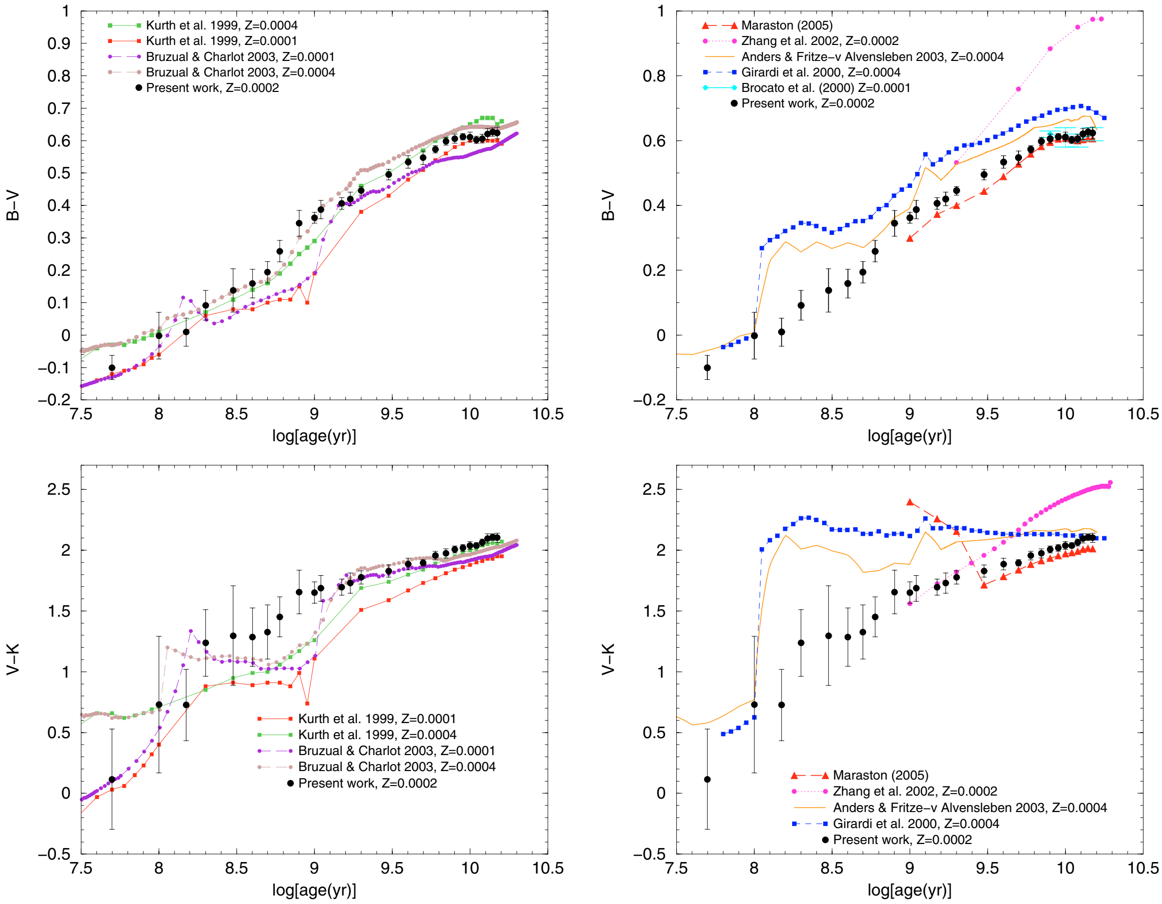

Fig. 6. Integrated colours ($B-V$, *upper panels*; $V-K$, *lower panels*) from recent papers: present models (black dots); Kurth et al. (1999, red $Z = 0.0001$, green $Z = 0.0004$ squares, solid line), Brocato et al. (2000, cyan dots), Anders & Fritze-v. Alvensleben (2003, orange solid line), Girardi et al. (2000, blue squares, short-dashed line), Zhang et al. (2002, pink circles, dotted line), Bruzual & Charlot (2003, violet $Z = 0.0001$, brown $Z = 0.0004$ circles, dashed line). Maraston (2005, red triangles, dashed line).

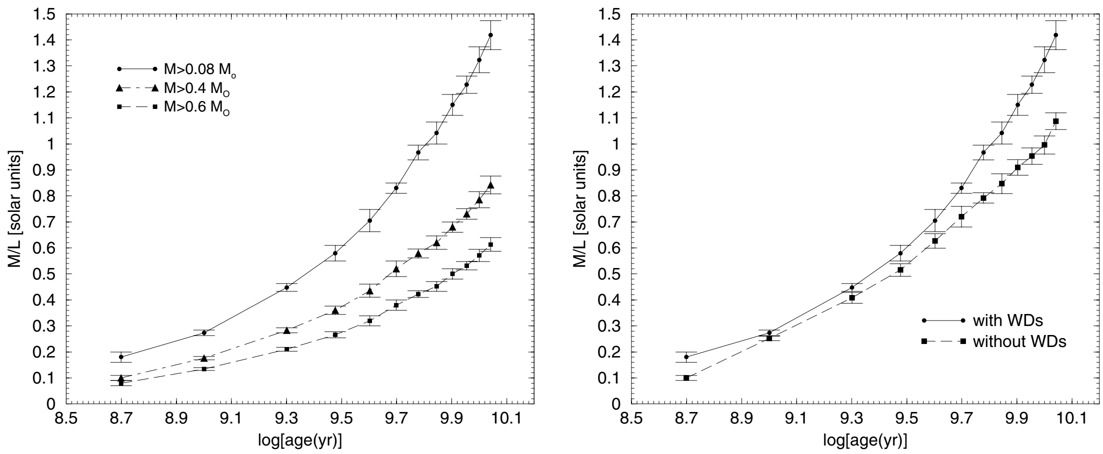

Fig. 7. *Left panel*: fraction of very low-mass stars ($M \le 0.6\,M_\odot$) that contribute to the mass-luminosity ratio (M/L) (in solar units) as a function of the age for $M_V^{\rm tot} = -8$. Filled circles represent our *standard* model in which all masses with $M \ge 0.08\,M_\odot$ are included; the effect of considering only stars with $M \ge 0.4\,M_\odot$ (filled triangles) or $M \ge 0.6\,M_\odot$ (filled squares) is analysed separately. *Right panel*: as in the left panel, but when the WD population is (filled circles, *standard* model) or is not (filled squares) included.

shows that the fraction of low-mass stars and white dwarfs increases with the cluster age (see also Maraston 1998). Since the simulations are performed at fixed absolute visual magnitude, the total mass of the cluster varies with age, as shown in Fig. 8, where we plot the case of $M_V = -8$. This is because, as the age increases, the mass of the typical star in the cluster decreases.

Changing $M_{\rm up}$ affects the number of stars cooling as WDs, or in other words the mass fraction locked as WDs, and thus the total mass of the cluster. Different input ingredients of stellar evolutionary tracks, as e.g. the neutrino energy losses in the core, lead to different predictions of $M_{\rm up}$ at fixed metallicity, see e.g. Tornambe & Chieffi (1986, $M_{\rm up} = 5.7\,M_\odot$), Pols et al. (1998,

Table 5. Mass-to-light ratios for selected ages in several photometric passbands from our *standard* model with different assumptions for $M_{\rm up}$.

	M/L_V	M/L_U	M/L_B	M/L_R	M/L_I	M/L_J	M/L_K
$M_{\rm up} = 5\,M_\odot$							
500 Myr	0.21 ± 0.01	0.126 ± 0.003	0.139 ± 0.004	0.25 ± 0.02	0.28 ± 0.04	0.28 ± 0.06	0.26 ± 0.08
800 Myr	0.28 ± 0.02	0.194 ± 0.007	0.210 ± 0.008	0.31 ± 0.03	0.31 ± 0.04	0.29 ± 0.05	0.25 ± 0.06
3 Gyr	0.66 ± 0.03	0.55 ± 0.01	0.58 ± 0.02	0.67 ± 0.03	0.64 ± 0.03	0.58 ± 0.04	0.50 ± 0.04
10 Gyr	1.55±0.04	1.45 ± 0.02	1.58 ± 0.03	1.47 ± 0.04	1.33 ± 0.05	1.15 ± 0.05	0.95 ± 0.05
$M_{\rm up} = 6.5\,M_\odot$							
500 Myr	0.22 ± 0.01	0.127 ± 0.003	0.140 ± 0.004	0.26 ± 0.02	0.28 ± 0.03	0.29 ± 0.06	0.26 ± 0.08
800 Myr	0.28 ± 0.01	0.191 ± 0.005	0.207 ± 0.006	0.30 ± 0.02	0.30 ± 0.03	0.28 ± 0.05	0.25 ± 0.06
3 Gyr	0.66 ± 0.03	0.55 ± 0.01	0.58 ± 0.02	0.67 ± 0.03	0.64 ± 0.04	0.58 ± 0.04	0.49 ± 0.04
10 Gyr	1.58 ± 0.05	1.47 ± 0.02	1.60 ± 0.03	1.49 ± 0.05	1.36 ± 0.06	1.17 ± 0.06	0.97 ± 0.06
$M_{\rm up} = 10\,M_\odot$							
500 Myr	0.22 ± 0.01	0.130 ± 0.002	0.143 ± 0.003	0.26 ± 0.02	0.28 ± 0.04	0.28 ± 0.06	0.26 ± 0.08
800 Myr	0.29 ± 0.01	0.199 ± 0.005	0.214 ± 0.005	0.31 ± 0.02	0.31 ± 0.03	0.29 ± 0.05	0.25 ± 0.05
3 Gyr	0.68 ± 0.03	0.56 ± 0.01	0.60 ± 0.02	0.69 ± 0.04	0.66 ± 0.04	0.60 ± 0.04	0.51 ± 0.05
10 Gyr	1.58 ± 0.05	1.48 ± 0.02	1.61 ± 0.04	1.49 ± 0.06	1.35 ± 0.06	1.16 ± 0.06	0.96 ± 0.06

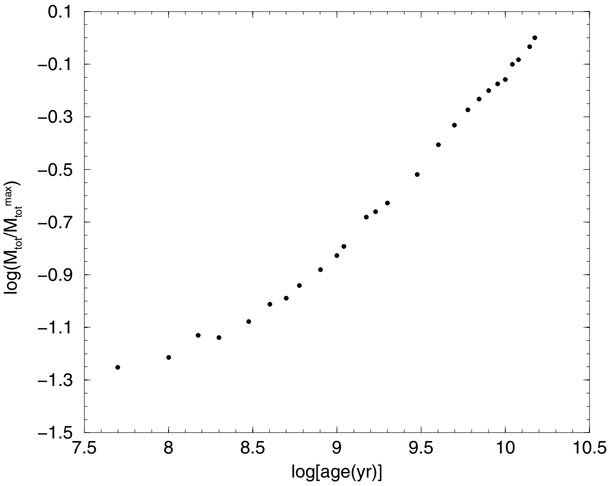

Fig. 8. Time behaviour of the logarithm of the cluster total mass needed to reach $M_V^{\rm tot} = -8$ normalized to the maximum value, as a function of age.

$M_{\rm up} = 5\,M_\odot$), Dominguez et al. (1999, $M_{\rm up} = 6.5\,M_\odot$), Cariulo et al. (2004, $M_{\rm up} = 5 \div 6\,M_\odot$). We explore the effect of changing $M_{\rm up}$. We find that increasing $M_{\rm up}$ from 5 up to 7 $M_\odot$ does not cause variations in the mass-to-light ratios, at least for the adopted IMF. Even pushing $M_{\rm up}$ up to 10 $M_\odot$ does not change the mass-to-light ratios significantly (Table 5).

5.1. $M_V^{\rm tot}$ sensitivity

Figure 9 shows the time evolution of $\mathcal{M}/L$ ratio in selected passbands for *standard* models with $M_V^{\rm tot} = -8$ (Table 6) and −4 mag. The corresponding data tables for the case of $M_V^{\rm tot} = -4$ and −6 are available at the CDS. Note that the mass-to-light ratios generally increase with age independently of the photometric band, because the total mass increases. This result is similar to what has been obtained by other authors, who do not keep the luminosity L_V constant (see e.g. Bruzual & Charlot 2003; Maraston 2005).

The only effect of changing the absolute magnitude from $M_V = -8$ to −4 on mass-to-light ratios in the optical bands is to increase the intrinsic uncertainties. In contrast, other than this effect mass-to-light ratios in the NIR bands suffer a larger scatter due to the decrease in red giant contributors to the total NIR luminosity, as shown in the right lower panel of the figure for K-band.

Since $M_V^{\rm tot}$ is fixed, the behaviour of $(\mathcal{M}/L_V)$ as a function of the age reflects the trend of the cluster mass (Fig. 8); it is quite linear for ages ≥1 Gyr in all passbands indicating it is driven by the growth in the total mass. For ages ≤1 Gyr, NIR colours are flatter than the optical (U, B, V) ones due to the increase in the infrared luminosity following the development of an extended AGB. We also find a dimming in $\mathcal{M}/L_K$ at the age corresponding to the AGB phase-transition confirming the result found by Maraston (2005) for higher metallicity.

Finally, Fig. 10 compares the present values with the ones by Bruzual & Charlot (2003), Anders & Fritze-v. Alvensleben (2003), and Maraston (2005) in two photometric bands, namely B and K. Concerning the B-band, the agreement with Bruzual & Charlot (2003) and Maraston (2005) is very satisfactory, while Anders & Fritze-v. Alvensleben (2003) predict slightly higher values at log age $\gtrsim$ 8.5.

A more complex behaviour is shown by $\mathcal{M}/L_K$: at log age $\gtrsim$ 9.3 the $\mathcal{M}/L_K$ is independent of the model, but model-dependent at younger ages. This reflects the great uncertainties in simulating the AGB phase we have already discussed for colours.

5.2. IMF variations

To evaluate the effect of the IMF shape on $\mathcal{M}/L$, we changed the IMF exponents within the estimated uncertainty (Kroupa 2002). Figures 11 and 12 show the effect of changing the IMF exponents with respect to the Kroupa formulation for masses higher and lower than 0.5 $M_\odot$, respectively. Models with $M_V^{\rm tot} = -8$ mag are plotted in selected passbands while results for other passbands, and for $M_V^{\rm tot} = -4$ mag are available at the CDS.

The $\mathcal{M}/L$ ratio is more sensitive than integrated colours to the IMF shape, as already noted by Maraston (1998), Bruzual & Charlot (2003), and Maraston (2005). From Fig. 11 it is evident that, by decreasing the IMF slope at $M \leq 0.5\,M_\odot$, the mass of the system decreases, while the luminosity remains almost constant. The final effect is to have lower $\mathcal{M}/L$ ratios than in the *standard* models ($\alpha = 1.3$). At age lower than few billion years, the uncertainty due to stochastic effects is comparable or larger than the effects of exponent variations. Indeed, the IMF variations can be appreciated at ages of the order of 10^{10} yr. We also find that the uncertainty predicted for $M_V^{\rm tot} = -4$ models prevents of any detection of significant variations at any age.

Table 6. Theoretical $\mathcal{M}/L$ as a function of the age in different photometric bands (solar units) obtained for *standard* models with $M_V^{\rm tot} = -8$. (Full version available at CDS.)

Age (Myr)	$\mathcal{M}/L_V$	$\mathcal{M}/L_U$	$\mathcal{M}/L_B$	$\mathcal{M}/L_R$	$\mathcal{M}/L_I$	$\mathcal{M}/L_J$	$\mathcal{M}/L_K$
50.	0.12 ± 0.01	0.032 ± 0.003	0.06 ± 0.01	0.17 ± 0.02	0.24 ± 0.05	0.4 ± 0.1	0.5 ± 0.2
100.	0.13 ± 0.02	0.046 ± 0.003	0.07 ± 0.01	0.18 ± 0.04	0.22 ± 0.07	0.3 ± 0.1	0.3 ± 0.2
150.	0.16 ± 0.01	0.061 ± 0.003	0.088 ± 0.005	0.21 ± 0.02	0.26 ± 0.04	0.33 ± 0.08	0.3 ± 0.1
200.	0.16 ± 0.01	0.070 ± 0.002	0.092 ± 0.003	0.19 ± 0.01	0.22 ± 0.03	0.23 ± 0.05	0.21 ± 0.06
300.	0.18 ± 0.01	0.091 ± 0.004	0.110 ± 0.005	0.22 ± 0.03	0.24 ± 0.05	0.25 ± 0.08	0.24 ± 0.10
400.	0.20 ± 0.01	0.109 ± 0.003	0.124 ± 0.005	0.24 ± 0.02	0.26 ± 0.04	0.27 ± 0.05	0.25 ± 0.06
500.	0.22 ± 0.01	0.127 ± 0.003	0.140 ± 0.004	0.25 ± 0.02	0.28 ± 0.03	0.29 ± 0.06	0.26 ± 0.08
600.	0.23 ± 0.02	0.148 ± 0.005	0.16 ± 0.01	0.27 ± 0.02	0.28 ± 0.03	0.28 ± 0.05	0.25 ± 0.06
800.	0.28 ± 0.01	0.191 ± 0.005	0.21 ± 0.01	0.30 ± 0.02	0.30 ± 0.03	0.28 ± 0.05	0.25 ± 0.05
1000.	0.33 ± 0.01	0.23 ± 0.01	0.25 ± 0.01	0.35 ± 0.01	0.35 ± 0.02	0.33 ± 0.02	0.29 ± 0.03
1100.	0.34 ± 0.02	0.24 ± 0.01	0.26 ± 0.01	0.36 ± 0.03	0.36 ± 0.03	0.33 ± 0.04	0.29 ± 0.04
1500.	0.43 ± 0.02	0.32 ± 0.01	0.35 ± 0.01	0.46 ± 0.02	0.45 ± 0.03	0.42 ± 0.03	0.37 ± 0.03
1700.	0.47 ± 0.02	0.36 ± 0.01	0.38 ± 0.01	0.49 ± 0.03	0.48 ± 0.03	0.45 ± 0.04	0.39 ± 0.05
2000.	0.52 ± 0.01	0.40 ± 0.01	0.43 ± 0.01	0.53 ± 0.02	0.52 ± 0.02	0.47 ± 0.03	0.40 ± 0.03
3000.	0.66 ± 0.03	0.54 ± 0.01	0.59 ± 0.02	0.67 ± 0.03	0.64 ± 0.04	0.58 ± 0.04	0.49 ± 0.04
4000.	0.81 ± 0.04	0.69 ± 0.02	0.74 ± 0.03	0.80 ± 0.05	0.75 ± 0.05	0.68 ± 0.05	0.57 ± 0.05
5000.	0.99 ± 0.05	0.84 ± 0.02	0.92 ± 0.03	0.97 ± 0.06	0.91 ± 0.06	0.82 ± 0.07	0.70 ± 0.07
6000.	1.12 ± 0.03	0.97 ± 0.01	1.08 ± 0.02	1.09 ± 0.03	1.01 ± 0.03	0.89 ± 0.03	0.76 ± 0.03
7000.	1.22 ± 0.04	1.09 ± 0.02	1.21 ± 0.03	1.17 ± 0.05	1.08 ± 0.05	0.94 ± 0.05	0.80 ± 0.05
8000.	1.36 ± 0.04	1.22 ± 0.02	1.36 ± 0.03	1.30 ± 0.05	1.18 ± 0.05	1.03 ± 0.05	0.86 ± 0.05
9000.	1.45 ± 0.03	1.33 ± 0.02	1.47 ± 0.02	1.38 ± 0.04	1.26 ± 0.04	1.09 ± 0.04	0.91 ± 0.04
10 000.	1.58 ± 0.05	1.47 ± 0.02	1.60 ± 0.03	1.49 ± 0.05	1.36 ± 0.06	1.17 ± 0.06	0.97 ± 0.06
11 000.	1.69 ± 0.06	1.58 ± 0.04	1.71 ± 0.05	1.61 ± 0.06	1.46 ± 0.06	1.25 ± 0.06	1.04 ± 0.05
12 000.	1.80 ± 0.07	1.69 ± 0.04	1.83 ± 0.06	1.70 ± 0.07	1.54 ± 0.07	1.31 ± 0.07	1.08 ± 0.07
13 000.	1.86 ± 0.09	1.78 ± 0.05	1.93 ± 0.07	1.74 ± 0.09	1.57 ± 0.09	1.33 ± 0.09	1.08 ± 0.08
14 000.	1.99 ± 0.07	1.92 ± 0.04	2.09 ± 0.06	1.86 ± 0.07	1.67 ± 0.07	1.41 ± 0.07	1.15 ± 0.07
15 000.	2.13 ± 0.07	2.04 ± 0.03	2.25 ± 0.06	1.99 ± 0.08	1.78 ± 0.09	1.51 ± 0.09	1.24 ± 0.09

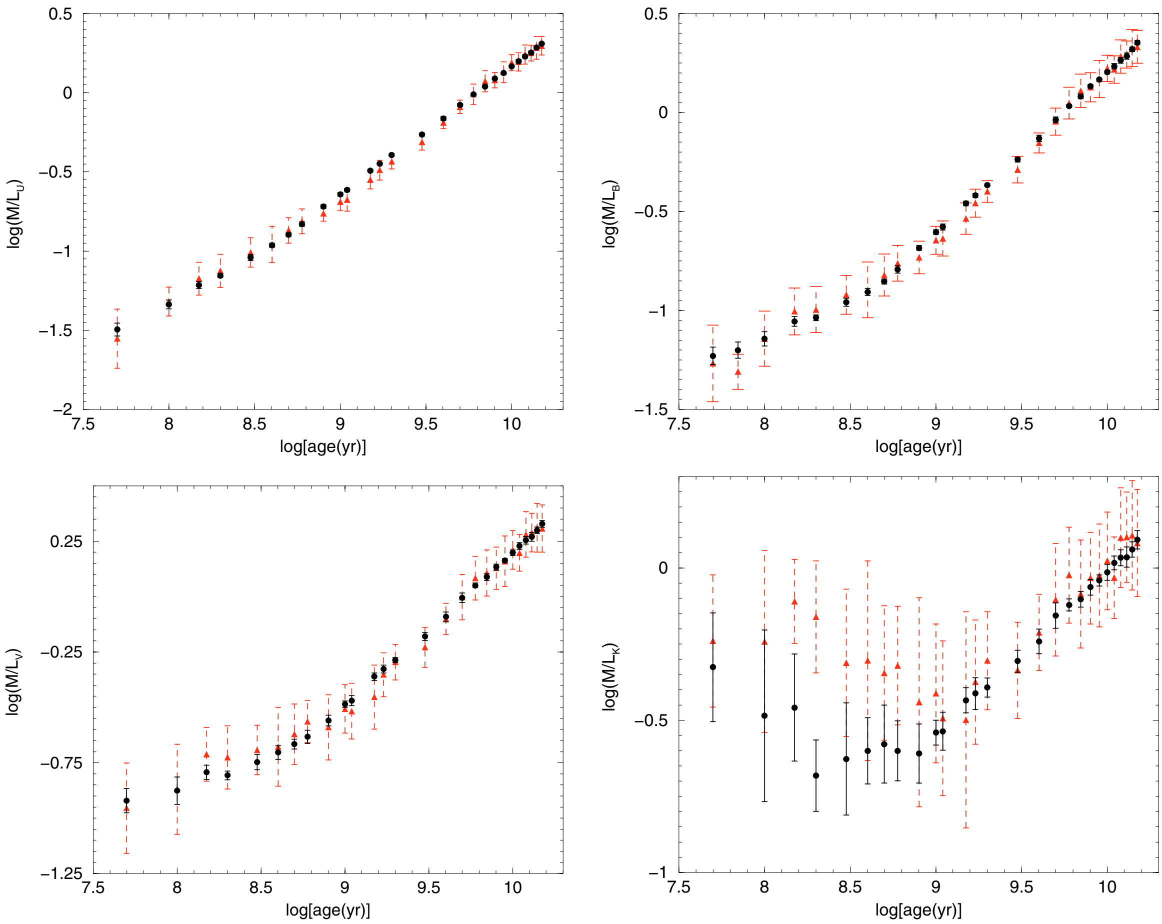

Fig. 9. Time behaviour of the $\mathcal{M}/L$ ratio (in solar units) for selected passbands (U, B, V, K). For each model, 1σ dispersion is shown. Red triangles (dashed line) indicate models with $M_V^{\rm tot} = -4$, and black dots (continuos line) models with $M_V^{\rm tot} - 8$.

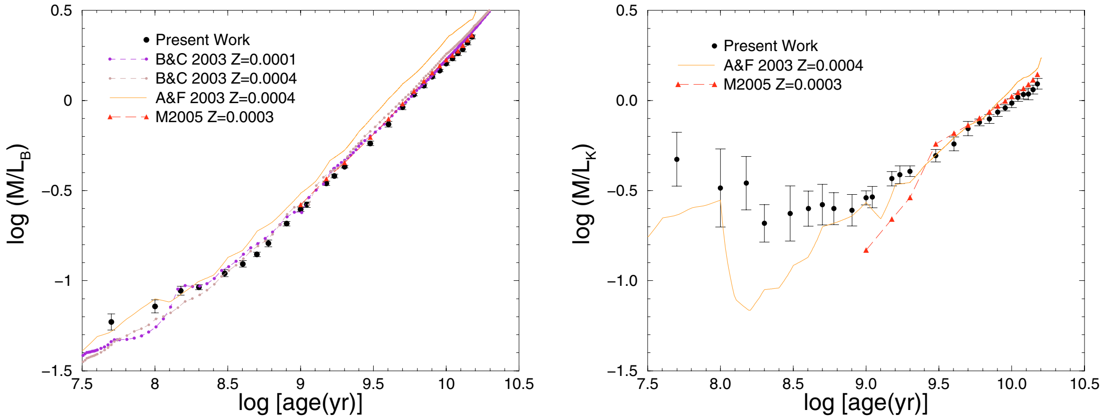

Fig. 10. Time evolution of $\mathcal{M}/L_B$ (*left panel*) and $\mathcal{M}/L_K$ (*right panel*) in our reference model (black dots) compared with the Bruzual & Charlot (2003, B&C 2003) for models with $Z = 0.0001$ (violet dashed line), and $Z = 0.0004$ (brown dashed line), Anders & Fritze-v. Alvensleben (2003, A&F 2003) models (orange solid line), and Maraston (2005, M2005) for $Z = 0.0003$ (red triangles, dashed line). The IMF adopted by various authors are reported in Table 4.

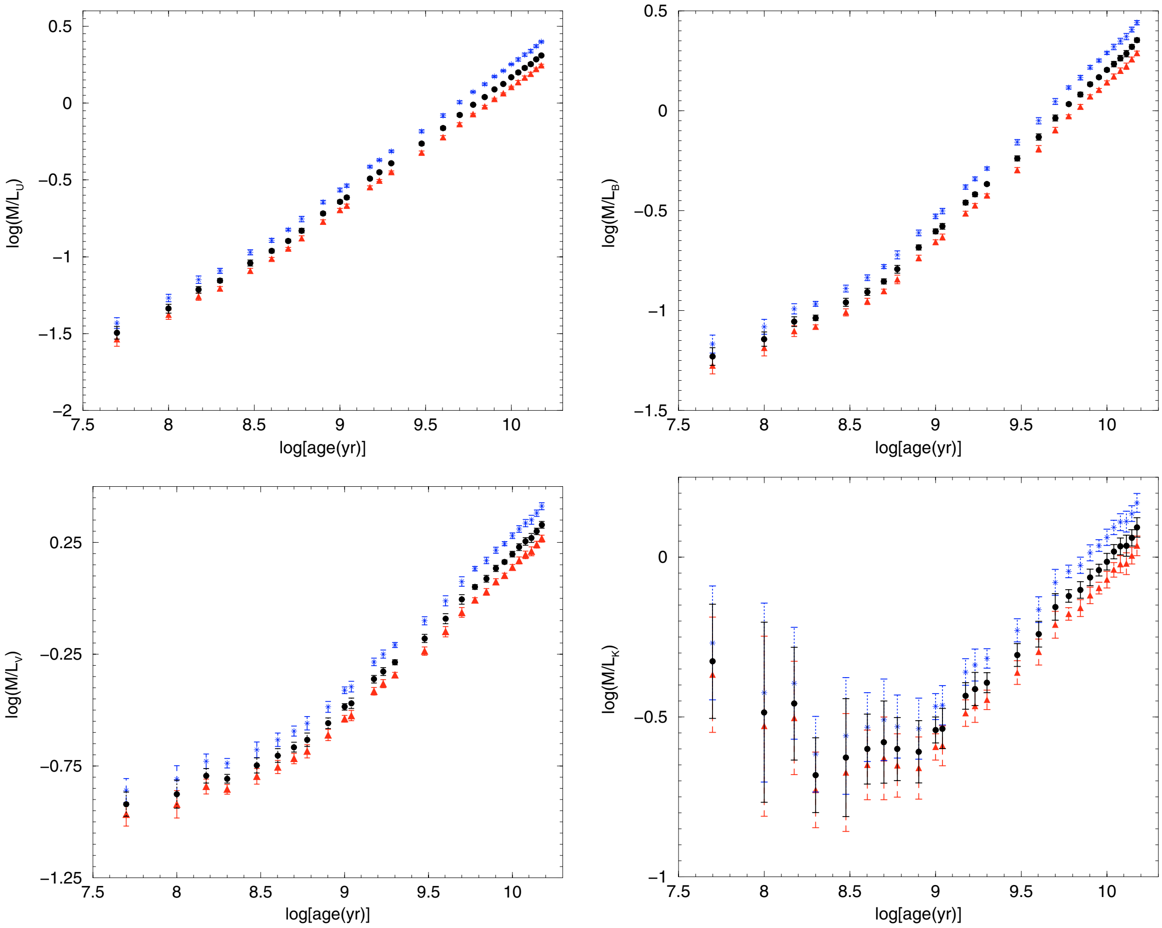

Fig. 11. Time evolution of $\mathcal{M}/L$ (in solar units) in selected passbands (U, B, V, K) for models with $M_V^{\rm tot} = -8$ calculated with the lower, central, and upper values for the Kroupa (2002) IMF exponent for $M \leq 0.5\ M_{\odot}$. Black dots indicate our reference model ($\alpha = 1.3$), red triangles indicate models with $\alpha = 0.8$, and blue stars models with $\alpha = 1.8$.

A different situation is found in Fig. 12. The $\mathcal{M}/L$ slightly depend on IMF for ages younger than a few billion years, while they are nearly insensitive at old age. This is because an IMF flatter than $\alpha = 2.3$ at $M \geq 0.5$ requires a total mass lower than in the *standard* case ($\alpha = 2.3$) to reach the given luminosity, thus predicting low $\mathcal{M}/L_V$. The effect is enhanced in young stellar populations in which the total mass is dominated by massive stars. On the other hand, by increasing the exponent up to 2.6, the cluster mass needed to have $M_V = -8$ increases, leading to high $\mathcal{M}/L$ values. Again, $\mathcal{M}/L$ in the NIR bands are more affected by stochastic phenomena.

Finally, note that in the case of small variations ($\alpha = 2 \div 2.6$) explored here, the contribution of massive remnants to the total mass does not change significantly, while it is shown to be effective if large variations ($\alpha = 0.5 \div 3.5$) are adopted, see the discussion in Maraston (1998).

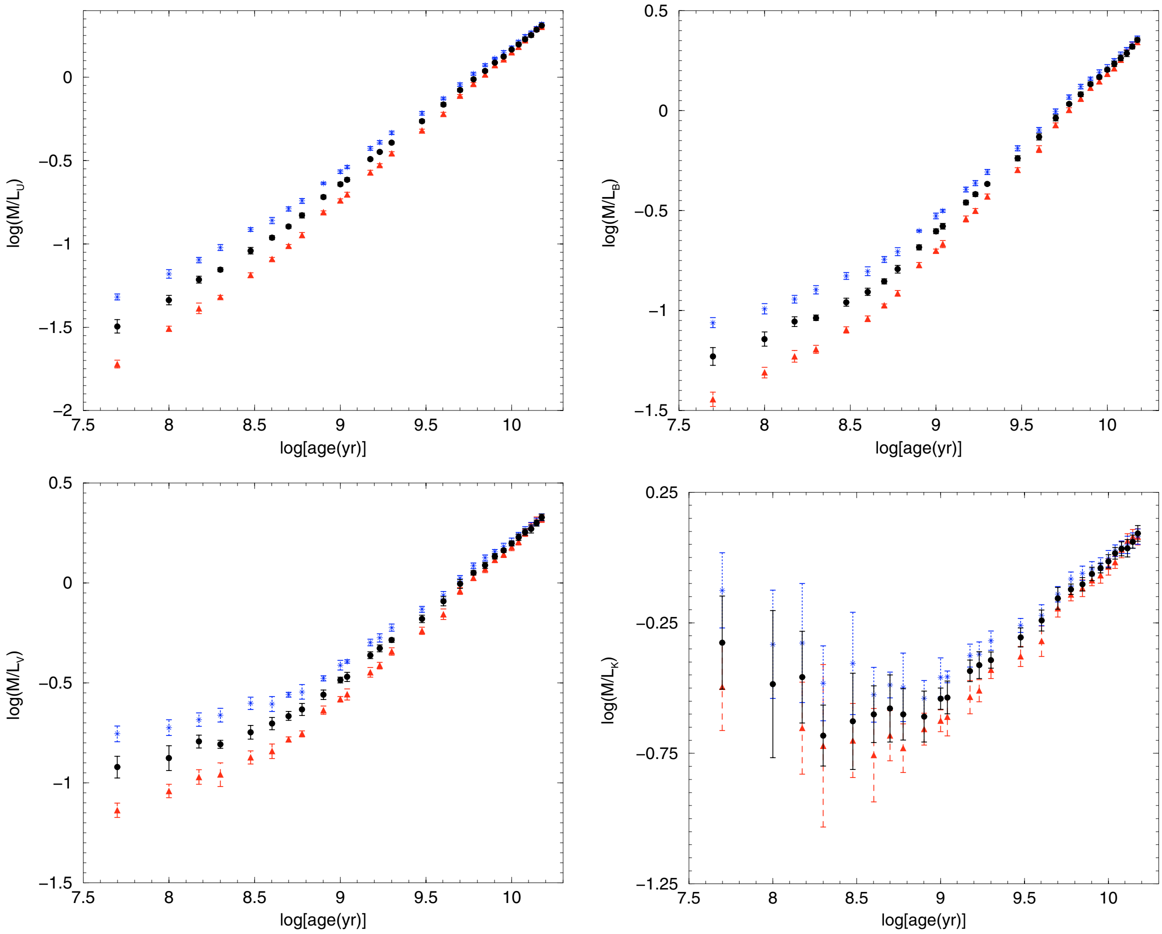

Fig. 12. Time evolution of $\mathcal{M}/L$ (in solar units) in selected passbands (U, B, V, K) for models with $M_V^{\rm tot} = -8$ calculated with the lower, central, and upper values for the Kroupa (2002) IMF exponent for $M \geq 0.5\ M_\odot$. Black dots indicate our reference model ($\alpha = 2.3$), red triangles indicate models with $\alpha = 2.0$, and blue stars indicate models with $\alpha = 2.6$.

6. Summary and conclusions

In this work we have analysed the intrinsic uncertainties due to stochastic effects on integrated colours and $\mathcal{M}/L$ of metal-poor stellar clusters as a function of the total visual magnitude. The calculations were performed for three different values of $M_V^{\rm tot}$ and for a fine grid of stellar ages. Statistical errors are shown to be crucial; especially in the extreme case $M_V^{\rm tot} = -4$, they are high enough to prevent precise quantitative evaluations for all ages. Calculations were made in the standard *UBVRIJHK* photometric passbands and in the Hubble Space Telescope bands (WFPC2 and NICMOS systems).

We checked the consistency of our models on the observational properties of three metal poor clusters, namely M 68, M 15, and M 30, which mainly differ in their absolute visual magnitude and HB morphology. For each cluster we were able to reproduce both the features of the observed CMD and the integrated colours, showing that the HB morphology does not influence the photometric indices being considered.

The comparison with recent results available in the literature shows, in some cases, non-negligible differences due to the wide variety of prescriptions used in the model calculations.

The uncertainties in the results on both colours and mass-to-light ratios due to the still present uncertainty on the IMF shape were quantitatively estimated; and while the colour fluctuations remain within theoretical uncertainties, the $\mathcal{M}/L$ ratio is more sensitive to the IMF shape. We also showed that the influence on $\mathcal{M}/L$ of the adopted value for the minimum mass for which carbon burning is ignited is quite negligible.

Acknowledgements. This work is dedicated to the memory of Vittorio Castellani, whose advise always supported us, and whose enthusiasm and dedication in challenging the astrophysics questions are an invaluable example for all of us. We warmly thank E. Brocato, P.G. Prada Moroni, and S.N. Shore for useful discussions and for a careful reading of the manuscript. We are grateful to the anonymous referee for her/his suggestions and comments that greatly improved the paper. Financial support for this work was provided by MIUR-COFIN 2003. This work made use of computational resources granted by the Consorzio di Ricerca del Gran Sasso according to the Progetto 6 *Calcolo Evoluto e sue Applicazioni (RSV6)*-Cluster C11/B. This paper utilises the HST-snapshot database by the Globular Cluster Group of the Padova Astronomy Department, and the Catalog of parameters for Milky Way Globular Clusters by W.E. Harris.

References

Allard, F., Hauschildt, P. H., Alexander, D. R., & Starrfield, S. 1997, ARA&A, 35, 137
Anders, P., & Fritze-v. Alvensleben, U. 2003, A&A, 401, 1063
Angeletti, L., Dolcetta, R., & Giannone, P. 1980, Ap&SS, 69, 45
Bailyn, C. D., Grindlay, J. E., Cohn, H., et al. 1989, AJ, 98, 882
Baraffe, I., Chabrier, G., Allard, F., & Hauschildt, P. H. 1997, A&A, 327, 1054
Baraffe, I., Chabrier, G., Allard, F., & Hauschildt, P. H. 1998, A&A, 337, 403
Barbaro, C., & Bertelli, C. 1977, A&A, 54, 243
Barmina, R., Girardi, L., & Chiosi, C. 2002, A&A, 385, 847
Baud, B., & Habing, H. J. 1983, A&A, 127, 73
Bergeron, P., Saumon, D., & Wesemael, F. 1995, ApJ, 443, 764
Bessell, M. S., Castelli, F., & Plez, B. 1998, A&A, 333, 231
Bloecker, T., & Schoenberner, D. 1997, A&A, 324, 991

Boily, C. M., Lançon, A., Deiters, S., & Heggie, D. C. 2005, ApJ, 620, L27
Bombaci, I., Parenti, I., & Vidaña, I. 2004, ApJ, 614, 314
Bressan, A., Chiosi, C., & Fagotto, F. 1994, ApJS, 94, 63
Brocato, E., Caputo, F., di Giorgio, A. M., Santolamazza, P., & Richichi, A. 1990a, Mem. Soc. Astron. It., 61, 137
Brocato, E., Matteucci, F., Mazzitelli, I., & Tornambe, A. 1990b, ApJ, 349, 458
Brocato, E., Castellani, V., Raimondo, G., & Romaniello, M. 1999, A&AS, 136, 65
Brocato, E., Castellani, V., Poli, F. M., & Raimondo, G. 2000, A&AS, 146, 91
Brocato, E., Castellani, V., Di Carlo, E., Raimondo, G., & Walker, A. R. 2003, AJ, 125, 3111
Bruzual, G., & Charlot, S. 2003, MNRAS, 344, 1000
Burstein, D., Faber, S. M., Gaskell, C. M., & Krumm, N. 1984, ApJ, 287, 586
Buzzoni, A. 1993, A&A, 275, 433
Cardelli, J. A., Clayton, G. C., & Mathis, J. S. 1989, ApJ, 345, 245
Cariulo, P., Degl'Innocenti, S., & Castellani, V. 2004, A&A, 421, 1121
Carretta, E., Gratton, R. G., Clementini, G., & Fusi Pecci, F. 2000, ApJ, 533, 215
Cassisi, S., Castellani, V., Ciarcelluti, P., Piotto, G., & Zoccali, M. 2000, MNRAS, 315, 679
Castellani, V., Chieffi, A., Tornambe, A., & Pulone, L. 1985, ApJ, 296, 204
Castellani, V., Degl'Innocenti, S., Marconi, M., Prada Moroni, P. G., & Sestito, P. 2003, A&A, 404, 645
Castelli, F. 1999, A&A, 346, 564
Castelli, F., Gratton, R. G., & Kurucz, R. L. 1997, A&A, 318, 841
Cerviño, M., & Luridiana, V. 2004, A&A, 413, 145
Cerviño, M., & Valls-Gabaud, D. 2003, MNRAS, 338, 481
Chabrier, G. 2003, PASP, 115, 763
Chabrier, G., & Baraffe, I. 1997, A&A, 327, 1039
Chabrier, G., & Mera, D. 1997, A&A, 328, 83
Charlot, S., & Bruzual, A. G. 1991, ApJ, 367, 126
Charlot, S., Worthey, G., & Bressan, A. 1996, ApJ, 457, 625
Chiosi, C., Bertelli, G., & Bressan, A. 1988, A&A, 196, 84
Ciacio, F., degl'Innocenti, S., & Ricci, B. 1997, A&AS, 123, 449
Cote, P., Marzke, R. O., & West, M. J. 1998, ApJ, 501, 554
De Marchi, G., & Paresce, F. 1994, ApJ, 422, 597
Di Criscienzo, M., Marconi, M., & Caputo, F. 2004, ApJ, 612, 1092
Dominguez, I., Chieffi, A., Limongi, M., & Straniero, O. 1999, ApJ, 524, 226
Fagiolini, M. 2004, Diploma Thesis, University of Pisa, Italy
Fellhauer, M., Lin, D. N. C., Bolte, M., Aarseth, S. J., & Williams, K. A. 2003, ApJ, 595, L53
Ferraro, F. R., Messineo, M., Fusi Pecci, F., et al. 1999, AJ, 118, 1738
Girardi, L., & Bertelli, G. 1998, MNRAS, 300, 533
Girardi, L., Bressan, A., Bertelli, G., & Chiosi, C. 2000, A&AS, 141, 371
Groenewegen, M. A. T., & de Jong, T. 1993, A&A, 267, 410
Harris, W. E. 1996, VizieR Online Data Catalog, 7195, 0
Harris, W. E. 2003, in A Decade of Hubble Space Telescope Science, ed. M. Livio, K. Noll, & M. Stiavelli, 78
Hurley, J. R., & Shara, M. M. 2003, ApJ, 589, 179
Kron, G. E., & Mayall, N. U. 1960, AJ, 65, 581
Kroupa, P. 2001, MNRAS, 322, 231
Kroupa, P. 2002, Science, 295, 82
Kroupa, P., Tout, C. A., & Gilmore, G. 1993, MNRAS, 262, 545
Kurth, O. M., Fritze-v. Alvensleben, U., & Fricke, K. J. 1999, A&AS, 138, 19
Kurucz, R. L. 1992, in The Stellar Populations of Galaxies, ed. B. Barbuy, & A. Renzini, IAU Symp., 149, 225
Larsen, S. S. 2000, MNRAS, 319, 893
Larsen, S. S., & Richtler, T. 1999, A&A, 345, 59
Lattanzio, J. C., & Wood, P. R. 2003, in Asymptotic giant branch stars, by Harm J. Habing and Hans Olofson. Astronomy and astrophysics library (New York, Berlin: Springer), 23
Lee, Y.-W., Demarque, P., & Zinn, R. 1994, ApJ, 423, 248
Lejeune, T., Cuisinier, F., & Buser, R. 1997, A&AS, 125, 229
Lejeune, T., Cuisinier, F., & Buser, R. 1998, A&AS, 130, 65
Maeder, A., & Zahn, J.-P. 1998, A&A, 334, 1000
Maraston, C. 1998, MNRAS, 300, 872
Maraston, C. 2005, MNRAS, 362, 799
Marigo, P., Girardi, L., & Bressan, A. 1999, A&A, 344, 123
Matteucci, A., Ripepi, V., Brocato, E., & Castellani, V. 2002, A&A, 387, 861
McNamara, B. J., Harrison, T. E., & Baumgardt, H. 2004, ApJ, 602, 264
Origlia, L., & Leitherer, C. 2000, AJ, 119, 2018
Palacios, A., Talon, S., Charbonnel, C., & Forestini, M. 2003, A&A, 399, 603
Pease, F. G. 1928, PASP, 40, 342
Peterson, C. J. 1993, in Structure and Dynamics of Globular Clusters, ed. S. G. Djorgovski, & G. Meylan, ASP Conf. Ser., 50, 337
Piotto, G., King, I. R., Djorgovski, S. G., et al. 2002, A&A, 391, 945
Pols, O. R., Schroder, K.-P., Hurley, J. R., Tout, C. A., & Eggleton, P. P. 1998, MNRAS, 298, 525
Prada Moroni, P. G., & Straniero, O. 2006, ApJ, in publication
Pryor, C., & Meylan, G. 1993, in Structure and Dynamics of Globular Clusters, ed. S. G. Djorgovski, & G. Meylan, ASP Conf. Ser., 50, 357
Raimondo, G., Brocato, E., Cantiello, M., & Capaccioli, M. 2005, AJ, 130, 2625
Reed, B. C. 1985, PASP, 97, 120
Reed, B. C., Hesser, J. E., & Shawl, S. J. 1988, PASP, 100, 545
Reimers, D. 1975, Mem. Soc. R. Sci. Liege, 8, 369
Renzini, A. 1992, in The Stellar Populations of Galaxies, ed. B. Barbuy, & A. Renzini, IAU Symp., 149, 325
Renzini, A., & Buzzoni, A. 1986, in Spectral Evolution of Galaxies, ed. C. Chiosi, & A. Renzini, ASSL 122, 195
Renzini, A., & Voli, M. 1981, A&A, 94, 175
Rey, S.-C., Yoon, S.-J., Lee, Y.-W., Chaboyer, B., & Sarajedini, A. 2001, AJ, 122, 3219
Richard, O., Michaud, G., & Richer, J. 2002, ApJ, 580, 1100
Richer, J., Michaud, G., Rogers, F., et al. 1998, ApJ, 492, 833
Rosenberg, A., Aparicio, A., Saviane, I., & Piotto, G. 2000, A&AS, 145, 451
Salaris, M., García-Berro, E., Hernanz, M., Isern, J., & Saumon, D. 2000, ApJ, 544, 1036
Salpeter, E. E. 1955, ApJ, 121, 161
Sandquist, E. L., Bolte, M., Langer, G. E., Hesser, J. E., & Mendes de Oliveira, C. 1999, ApJ, 518, 262
Santos, Jr., J. F. C., & Frogel, J. A. 1997, ApJ, 479, 764
Saumon, D., & Jacobson, S. B. 1999, ApJ, 511, L107
Scalo, J. M. 1986, Fundamentals of Cosmic Physics, 11, 1
Spitzer, L. 1987, Dynamical evolution of globular clusters (Princeton, NJ: Princeton University Press), 191
Stetson, P. B., & West, M. J. 1994, PASP, 106, 726
Straniero, O., Domínguez, I., Cristallo, R., & Gallino, R. 2003, PASA, 20, 389
Thoul, A. A., Bahcall, J. N., & Loeb, A. 1994, ApJ, 421, 828
Tornambe, A., & Chieffi, A. 1986, MNRAS, 220, 529
Vazdekis, A. 1999, ApJ, 513, 224
Vesperini, E., & Heggie, D. C. 1997, MNRAS, 289, 898
Wagenhuber, J., & Groenewegen, M. A. T. 1998, A&A, 340, 183
Walker, A. R. 1994, AJ, 108, 555
West, M. J., Côté, P., Marzke, R. O., & Jordán, A. 2004, Nature, 427, 31
Westera, P., Lejeune, T., Buser, R., Cuisinier, F., & Bruzual, G. 2002, A&A, 381, 524
Worthey, G. 1994, ApJS, 95, 107
Yi, S. K. 2003, ApJ, 582, 202
Zhang, F., Han, Z., Li, L., & Hurley, J. R. 2002, MNRAS, 334, 883
Zhang, F., Li, L., & Han, Z. 2005, MNRAS, 364, 503